THE RESPONSE OF ^{6}LiF AND ^{7}LiF THERMOLUMINESCENT DOSIMETERS TO NEUTRON AND GAMMA-RADIATION DOSE

by

CHARLES EDWARD BLISS

B. S., Kansas State University, 1967

A MASTER'S THESIS

submitted in partial fulfillment of the

requirements for the degree

MASTER OF SCIENCE

Department of Nuclear Engineering

KANSAS STATE UNIVERSITY
Manhattan, Kansas

1969

Approved by:

Major Professor

TABLE OF CONTENTS

LIST OF FIGURES

LIST OF TABLES

NOMENCLATURE

N	sample disintegrations during a counting time
ε_1	detector efficiency for photoelectric absorption of γ_1
ε_2	detector efficiency for photoelectric absorption of γ_2
ε_1'	detector total efficiency for photoelectric, Compton or pair production absorption of γ_1
ε_2'	detector total efficiency for photoelectric, Compton or pair production absorption of γ_2
A_1	area under γ_1 photopeak, counts
A_2	area under γ_2 photopeak, counts
A_{12}	area under the sum peak, counts
A	total area in the decay spectrum, counts
N_A	number of parent nuclei
N_B	number of daughter nuclei
λ_B	nuclide B characteristic decay constant, sec^{-1}
Φ	neutron flux, neutrons/cm^2, sec
σ	microscopic cross section, cm^2
$t_{\frac{1}{2}}$	half life of radioactive product, sec
t	irradiation time, sec
$\bar{t}$	corrected decay time, sec
t_m	mean life of radioactive product, sec
t_r	time from the removal from the neutron flux to the beginning of the count, sec
t_s	counting time, sec
L	Avogadro's constant, 6.02×10^{23} $mole^{-1}$

w	weight of activation foil, g
W_A	atomic weight of material A, g/mole
F	neutron fluence, neutrons/cm^2
TLD	thermoluminescent dosimeter
R.U.	TLD reader unit
R	dosimeter response, R.U.
R_o	dosimeter response due to constant Gammacell dose, R.U.
$\dot{R}$	Gammacell dose rate in response units, R.U./sec
D	gamma-photon dose received, R
D_o	constant Gammacell dose, R
$\dot{D}$	dose rate, R/sec
a	arbitrary constant, 10^9 neutrons/cm^2, R.U.
b	arbitrary constant, 10^9 neutrons/cm^2
Y_i	counts in channel i of photopeak
Y_o	count corresponding to channel x_o
x_o	mean channel of the Gaussian function
x_i	channel number
b_o	$2\sigma^2$
σ^2	variance of the Gaussian function
z_i	$\ln Y_i$
a_1	$\ln Y_o - x_o^2/b_o$
a_2	$2x_o/b_o$
a_3	$-1/b_o$
$\underline{a}$	(3 x 1) vector of the coefficients a_1, a_2, and a_3
n	number of channels

$\underline{X}$	(n x 3) matrix whose first column is composed of all unity values, the second column is composed of x_i values, and the third column is composed of the x_i^2 values
$\underline{X}'$	transpose of $\underline{X}$
$\underline{Z}$	(n x 1) vector of the z_i values
$\underline{W}$	(n x n) diagonal weighting matrix whose elements are the inverse of the variances of the z_i values
S_L	minimum total squared deviation in linearized domain
S_D	actual minimum total squared deviation
$\underline{C}$	inverse matrix of $\underline{X}' \underline{W} \underline{X}$
K_i	$\exp\{-(x_i - x_o)^2/b_o\}$

1. INTRODUCTION

Radiation dosimetry is the art of determining radiation dose by measuring the effects of radiation. Radiation dose refers to the amount of energy deposited in an absorbing material and is dependent on the type and energy of the radiation. The basic unit for radiation exposure due to gamma rays is the roentgen, defined as "that amount of x or gamma radiation such that the associated corpuscular emission per .001293 g of air produces, in air, ions carrying one electrostatic unit of quantity of electricity of either sign." A more useful unit of radiation dose is the rad, which is equivalent to 100 erg absorbed per gram in the material in which the absorption occurs.

Historically, the search for an ideal radiation dosimeter has been continuing since the discovery of ionizing radiation. For a long while the ionization chamber was the basis for all dosimetry until supplemented by photographic emulsions and chemical dosimetry. Recently, solid-state dosimetry has been shown to be quite promising. As given by Spurny[1], solid-state dosimetry is based upon any of the following phenomena:

a) radiocoloration or decoloration;

b) radiophotoluminescence effect;

c) radiothermoluminescence effect;

d) luminescence degradation;

e) miscellaneous effects, such as changes of conductivity, blackening of a photoemulsion, etc.

The thermoluminescence phenomenon has been the subject of much research. Thermoluminescent dosimeters (TLD's) have been developed that have a number of advantages. They are useful over a wide range of dose (10^{-4} to 10^{6}R) and are sensitive to alpha, beta, gamma, neutron and proton radiation. They are small in size, precise, easily read, and reusable. The only drawbacks are that they require calibration prior to use in unknown radiation fields, they are sensitive to impurities and therefore quite difficult to reproduce, and the reader equipment is complicated and expensive. Thermoluminescent dosimeters have found use in the fields of health physics, space exploration, radiobiology, radiotherapy, civil defense and industry. A list of materials exhibiting thermoluminescent properties is given in ref. (1).

Thermoluminescent dosimetry utilizing LiF was first developed by Daniels[2]. Lithium-fluoride thermoluminescent phosphors are available in three forms and are manufactured by the Harshaw Chemical Company. TLD-100 (natural LiF) is composed of 92.5% ^{7}Li isotopic abundance. TLD-600 is enriched to 95.62% in ^{6}Li. TLD-700 contains 99.99% ^{7}Li. TLD-600 and TLD-700 have been used in thermal neutron and gamma ray mixed field dosimetry[1,3,4,5]. The two types of dosimeters have nearly identical gamma responses, but TLD-700 is nearly insensitive to thermal neutrons. Above thermal energies, the neutron responses of TLD-600 and TLD-700 have been shown to be quite energy dependent[6].

The light emitted by a thermoluminescent material is proportional to the dose received, so calibration is required before light emitted from a dosimeter with unknown exposure can be empirically related to actual dose received. A calibration curve relating thermoluminescent response in relative light units to radiation dose is generally produced prior to experimentation in unknown radiation fields. It was the purpose of this research to determine calibration curves for ^{6}LiF and ^{7}LiF for gamma-radiation and fast-neutron dose, to compare these calibrations, and to determine the response characteristics of these two types of dosimeters to combined neutron and gamma-radiation dose. Studies of mixed radiation-field effects, dose-rate effects, temperature, annealing and other physical environment effects are important in gaining new insights of the thermoluminescence phenomenon.

2. THEORY

2.1. EXPLANATION OF SOLID-STATE TERMINOLOGY

2.1.1. Energy-band Model of a Crystal:

When two isolated atoms are brought together, their outer or valence electrons interact to bind the atoms together. The valence electrons of one atom are attracted to the nucleus of the other atom, and the energy required to replace an electron from one nucleus to the other is therefore reduced. A valence electron is equally likely to be near either of the nuclei, and there are two energy levels for electrons at each nucleus. When many thousands of atoms are brought together in a crystal, these energy levels merge into a single band called the valence band. The upper unoccupied energy levels of atoms are similarly split when a crystal is formed from isolated atoms, forming what is known as the conduction band. For a pure insulating crystal, the energy band model can be represented as shown in Fig. 1a.

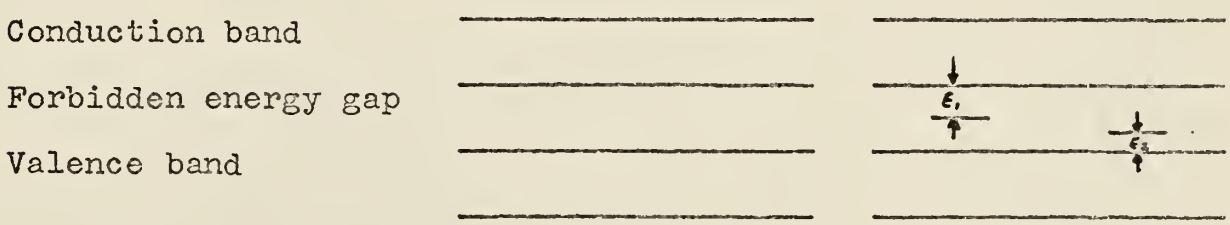

Fig. 1. Energy-band model of ideal and non-ideal crystals.

For a complete explanation of the energy-band model, the reader is referred to pertinent literature [7].

2.1.2. Traps:

Structural imperfections, such as vacancies, interstitials, or impurities, create centers of localized positive or negative charge within a crystal. A positive localized charge is capable of attracting and trapping an electron, and a localized negative charge is capable of attracting and trapping a positive hole. An electron trapped at an anionic vacancy is known as an F-center, and a hole trapped at a positive ion vacancy is known as a V-center. An F-center roughly resembles a hydrogen atom in which an electron is bound by the positive charge of the nucleus. Like the hydrogen atom, the F-center has certain discrete allowed energy levels and can make transitions between the various energy levels by absorption or emission of the proper quanta of energy. This energy of absorption or emission can be in the form of light quanta or as heat or vibrational energy. The possibility of absorbing light makes the crystal colored, and the traps which give rise to these absorptions are therefore also known as color centers.

2.1.3. Trap Depth:

Energetically, traps are located in the forbidden energy gap of a pure insulating crystal as shown in Fig. 1b. For a trapped electron, the trap depth is the energy difference between the trap and the bottom of the conduction band, E_1. For a trapped hole, the trap depth is the energy difference between the trap and the top of the valence band, E_2.

2.1.4. Phosphorescence:

Upon irradiation, certain insulating crystals containing various available traps store radiation-energy deposited by trapping electrons or holes or both. At a later time, they release this energy in the form of light photons. This general process is called phosphorescence.

2.1.5. Thermoluminescence:

At room temperature, there is a finite but small probability that traps will give rise to phosphorescence. This probability for release of trapped electrons and holes increases with increasing temperature. If the phosphorescence process is thus accelerated by increasing the temperature of the crystal, this phenomenon is known as thermoluminescence.

2.1.6. Phosphor:

A phosphor is a material which exhibits phosphorescence. The basis for a phosphor is a pure insulating crystal, but it is the irregularities in the crystal that are responsible for the phosphorescence.

2.1.7. Glow Curve:

As a phosphor is heated, the luminescence increases until nearly all the traps are emptied. A plot of the intensity of this light emitted vs. temperature or time is referred to as the glow curve.

2.2. THE PROCESS OF RADIATION THERMOLUMINESCENCE:

The process of radiation thermoluminescence involves several individual steps. First, the effect of radiation on a phosphor is to excite electrons from the filled valence band to the previously empty conduction band. Secondly, electrons from the conduction band fall into traps within the forbidden energy gap. If these traps are shallow, the electrons may receive enough thermal energy to escape from the traps at room temperature. This is the case in semiconductors, where the forbidden energy gap is narrow, and the traps are located only slightly below the conduction band. In phosphors, however, the traps are relatively deep, and the electrons have a very small probability of escape at room temperature. Trap depth, therefore, is one measure of the suitability of a phosphor for use as a thermoluminescent dosimeter. The number of filled traps in an irradiated phosphor is a function of the radiation dose received; it may also be a function of dose rate as well as other variables collectively termed radiation quality (type of radiation, energy, polarization). To determine the dose received, the phosphor is heated. As the temperature increases, the probability for escape of electrons increases, and as they escape, the electrons are again free to wander in the conduction band. Finally, these free electrons combine with free holes in the valence band or with trapped holes within the forbidden energy gap, giving off excess energy in the form of light photons. An analogous series of processes can also take place

wherein a trapped hole is thermally liberated from its trap and migrates through the valence band until it combines with a trapped or conduction band electron, emitting a photon in the process.

This is a reasonable but oversimplified explanation of thermoluminescence. The complicated nature of glow curves suggests that several different types of electron and hole traps exist, and their de-population mechanisms may be much more complicated.

2.3. THERMOLUMINESCENT DOSIMETRY

2.3.1. Use of a Phosphor as a Dosimeter:

Thermoluminescent dosimetry involves detection of the light emitted by a phosphor as a measure of the radiation received by the phosphor. The detection of the light photons which arise from the releasing of trapped electrons and holes is accomplished by a photomultiplier tube. The light detected by the P.M. tube is proportional to the number of filled traps which is in turn proportional (though not necessarily linearly proportional)[8] to the radiation dose absorbed by the crystal.

2.3.2. Useful properties of TLD materials:

In an excellent review article by Schulman [9], desirable properties of useful TLD materials are listed:

1) a high concentration of electron and hole traps;
2) high efficiency of luminescence when electrons or holes are thermally released and recombine;

3) long storage of trapped electrons and holes at normal working temperatures;

4) a simple trap distribution for greatest simplicity of operation and reading interpretation;

5) a luminescence spectrum which matches the detector and is separated as far as possible from the incandescent emission of the heating source;

6) stability of the phosphor to radiation (i.e., radiation should fill the traps but not create or destroy traps).

In addition to this list, Spurny[1] also specifies the following:

1) no excitation of phosphor other than by radiation;

2) linear response over range of dose;

3) cheap and reproducible production of the phosphor material.

2.3.3. The Effect of Impurities:

Several different types of traps are normally present in materials used for thermoluminescent dosimetry. Therefore, the glow curve may exhibit several peaks, and the emission spectrum may be quite complicated [10].

To control the emission spectrum of a phosphor for dosimetry use, it is often doped with known amounts of certain impurities. For instance, if silver, Ag, is used as an impurity, electron trapping leads to F-center formation as usual, but holes may be trapped at the Ag^+ ion. When an electron is excited from

an F-center to the conduction band, it combines with the hole at the Ag^+ ion and excites characteristic ultraviolet-blue Ag luminescence.

A divalent cation impurity can act as a possible electron trap because of its excess positive charge. Magnesium as an impurity has been shown to have important effects on the use of LiF as a dosimeter[10-12].

2.3.4. Use of LiF as a TLD:

LiF was among the first materials to be used as a TLD[2,13]. The thermoluminescence from LiF is unusually bright, and the coloration lies primarily in the ultraviolet range. Its tissue equivalence makes it ideal for use as a personnel dosimeter. The thermoluminescent response of LiF has very little dependence on photon energy[14] although the neutron response is known to be energy dependent[6].

As described in section 1, LiF is available in three different forms: TLD-100, containing natural LiF; TLD-600, containing primarily ^6Li; and TLD-700, containing primarily ^7Li.

A typical glow curve obtained from TLD-100 is shown in Fig. 2[15]. This curve is characterized by five peaks, as numbered in Fig. 2. The approximate temperatures at which the second and fifth peaks appear are 105°C and 190°C, respectively. All the peaks show some tendency to decay at room temperature, and the half lives of peaks 1 to 5 are 5 min., 10 hr., 0.5 yr.,

Fig. 2. Typical glow curve for TLD-100.
(Peaks 2 and 5 appeared at times in the heating cycle corresponding to 105°C and 190°C, respectively.)

7 yr., and 80 yr., respectively. Peak 5 is most suitable for LiF dosimetry.

The upper limit for LiF dosimetry is set by saturation effects that become pronounced at about 10^5 R. The lower limit of detectability is set by background dark current in the reader equipment and black body-radiation from the heater element.

2.4. FOIL-ACTIVATION DETERMINATION OF FAST-NEUTRON FLUENCE

2.4.1. Purpose:

When dealing with neutron dosimetry, it is often necessary to determine the neutron fluence (n/cm^2) at a given point in a reactor or near the target of a neutron producing accelerator. Such determinations are usually difficult and very often expensive. Methods in common use include proton recoil detectors, BF_3 probes, alpha detectors, and proton recoil counting in emulsions.

An accurate and inexpensive method for fluence measurement is the foil-activation technique. The initial activity of an activated foil is determined and related to the neutron flux by the solution of the appropriate differential equations for the production and decay of a specific radioisotope. This method requires that the activation cross section of the desired nuclear reaction be well known. The absolute activity of the irradited foil must be determined within reasonable statistical limits. The standard deviation of the flux, and therefore, the standard deviation of the fluence, depend on the accuracy of both the cross section and the absolute activity.

2.4.2. The Sum-Peak Method for Absolute Activity:

The sum-peak method was developed by Brinkman et al.[15]. It allows the determination of absolute activity within ± 5%[15].

For a radioisotope emitting two coincident gamma rays, the energy spectrum determined by a NaI(Tl) scintillation crystal detector is characterized by two prominent photoelectric peaks. Since there is a finite probability that the two gamma rays will be detected at the same time, a small "sum peak" will also appear at a point corresponding to the total energy of the two gamma rays.

For a given radioisotope, let N equal the disintegrations during a given counting time. Also define:

ε_1 = detector efficiency for photoelectric absorption of γ_1,

ε_2 = detector efficiency for photoelectric absorption of γ_2,

ε_1' = detector total efficiency for photoelectric, Compton or pair production absorption of γ_1,

ε_2' = detector total efficiency for photoelectric, Compton or pair production absorption of γ_2.

Then:

$$A_1 = N\varepsilon_1(1-\varepsilon_2') = \text{area under } \gamma_1 \text{ photopeak,} \qquad (2.4.2\text{-}1)$$

$$A_2 = N\varepsilon_2(1-\varepsilon_1') = \text{area under } \gamma_2 \text{ photopeak,} \qquad (2.4.2\text{-}2)$$

$$A_{12} = N\varepsilon_1\varepsilon_2 = \text{area under the sum peak.} \qquad (2.4.2\text{-}3)$$

The total area in the spectrum is

$$A = N - N(1-\varepsilon_1')(1-\varepsilon_2') \qquad (2.4.2\text{-}4)$$

where $(1-\varepsilon_1')(1-\varepsilon_2')$ is the probability that neither γ_1 nor γ_2

is detected. Equations (2.4.2-1) through (2.4.2-4) can be combined to give

$$N = A + \frac{A_1 A_2}{A_{12}} \qquad (2.4.2\text{-}5)$$

Equation (2.4.2-5) shows that the absolute activity of the radioisotope can be determined without information about the detector efficiencies.

2.4.3. Fluence Determination Using Foil Activity:

The absolute activity of a radioisotope can be related to the flux used in the irradiation of a sample. The solution of the well known differential equation for the production of isotope B from the neutron activation of isotope A is

$$N_B \lambda_B = \Phi \sigma N_A (1 - e^{-\lambda_B t}) \qquad (2.4.3\text{-}1)$$

where

N_A = number of parent nuclei,

N_B = number of daughter nuclei,

λ_B = decay constant for product B, sec^{-1},

Φ = neutron flux, neutrons/cm^2, sec,

σ = activation cross section for production of A from B, cm^2,

t = time of irradiation.

When the sample is removed from the neutron flux, the activity begins to decay and is given as a function of time by

$$N_B \lambda_B = \Phi \sigma N_A (1 - e^{-\lambda_B t}) e^{-\lambda_B \bar{t}} \qquad (2.4.3\text{-}2)$$

where $\bar{t}$ is the corrected decay time to account for decay of the sample during a finite counting time. $\bar{t}$ is given by

$$\bar{t} = t_r - t_m\{\ln[t_m(1-e^{-t_s/t_m})/t_s]\} \qquad (2.4.3\text{-}3)$$

where

t_r is the time from removal from the neutron flux to the beginning of the count,

t_s is the counting time,

$t_{\frac{1}{2}}$ is the half life of the radioactive product,

t_m is the mean life of the radioactive product ($t_{\frac{1}{2}}/\ln 2$).

The product of Eq. (2.4.3-2) and t_s is the disintegrations of the sample in the counting time. This is also given by Eq. (2.4.2-5). This equality gives the following relation for the neutron flux:

$$\Phi = \frac{(\frac{A_1 A_2}{A_{12}} + A)\, e^{\lambda_B \bar{t}}}{N_A(1-e^{-\lambda_B t})t_s} \qquad (2.4.3\text{-}4)$$

The number of parent nuclei is given by the product of Avogadro's constant and the weight of the sample, w, divided by the atomic weight, W_A of material A.

$$N_A = \frac{Lw}{W_A} \qquad (2.4.3\text{-}5)$$

where L is Avogadro's constant, 6.02×10^{23} mole^{-1}.

The fluence is given by the product of the flux and the irradiation time:

$$F = \frac{\left(\frac{A_1 A_2}{A_{12}} + A\right) e^{\lambda_B t} W_A t}{Lw(1-e^{-\lambda_B t})t_s} \qquad (2.4.3\text{-}6)$$

2.4.4. Curve-Fitting Technique for the Sum-Peak Method:

The main source of error in determination of the absolute activity by the sum-peak method is the evaluation of the areas under the three peaks. This difficulty led Brinkman *et al.*[15] to conclude that the absolute activity could be determined with only a ±5% precision.

By a method described in Appendix A, it was possible to use a least-squares analysis to fit the photopeaks to a Gaussian curve. This allowed determination of the absolute activity of activation foils within a ±3% precision.

3. FACTORS AFFECTING LiF THERMOLUMINESCENCE

3.1. PREIRRADIATION ANNEALING

3.1.1. Necessity for Preirradiation Annealing:

Following irradiation and readout, it is necessary that LiF be annealed to insure that all traps are emptied. As shown by Zimmerman et al.[16], the method of annealing has marked effect on the subsequent readout of irradiated LiF. For consistency, it is therefore necessary to decide upon and adhere to a suitable annealing procedure.

3.1.2. Suggested Preirradiation Annealing Methods:

For the TL-22 and TL-23 dosimeters used in this research (see section 4.1 for description), ref. (8) suggests a primary annealing such as 1 hour at 350°C or 400°C followed by a 24 hour annealing at 80°C. Zimmerman et al.[16] studied the effects of preirradiation annealing on TLD-100 and reported that annealing for 1 hour at 400°C removes all effects of previous annealing, and that annealing at 400°C beyond 1 hour has little effect on the glow curve. They also recommended an 80°C annealing for 24 hours following the 400°C annealing to reduce peaks 1 and 2 (Fig. 2) relative to the higher temperature peaks.

The low-temperature peaks can also be reduced by a postirradiation partial annealing (see section 3.2.2). Kaiseruddin[17] investigated the effect of eliminating the 24 hour 80°C annealing and reported no significant change in standard deviation of the response values. Therefore, Kaiseruddin[17] adopted the 400°C annealing procedure for TLD-100.

Since the chemical and crystal structure of TLD-600 and TLD-700 are similar to that of TLD-100, the same results were assumed to hold true for TLD-600 and TLD-700, and the same 400°C annealing procedure was adopted for this research.

3.2. POSTIRRADIATION ANNEALING

3.2.1. Purpose:

To function as a satisfactory dosimeter, a phosphor should have a thermoluminescent response that is independent of the storage time prior to readout. Fading effects in LiF have been studied by Endres[4] who reported a 5% decrease in the total light output over a period of 15 days. Karzmark *et al*[18] reported a 10% to 20% decrease in total light output over a period of 3 weeks followed by an increase toward the initial value in 6 to 8 weeks. This fading effect is probably due to the thermal release of lower-temperature traps at room temperature. This release leads to two effects:

1) a reduction in the total light output due to reduction in height of lower-temperature peaks;
2) an increase in the height of high temperature peaks caused by a fraction of the electrons released from low temperature traps falling from the conduction band into high temperature traps.

Therefore, for consistent results, it is necessary to remove these lower-temperature peaks by a standardized method, since their random decay can lead to inconsistencies.

3.2.2. Suggested Methods of Postirradiation Annealing:

Cameron et al.[19] reported that low temperature peaks could be removed by postirradiation annealing at 100°C for 10 minutes. Dean and Larkins[20] reported annealing the dosimeters at 110°C for 7 minutes, approximately 1 hour after the irradiation. This latter technique was investigated and is reported in section 5.1.

3.3. TYPE OF RADIATION:

The type of radiation has marked effect on the creation and readout of traps in LiF. Such effects must be well known before a dosimeter is used in a mixed radiation field.

3.3.1. Effect on Production of F-centers:

The energy required to produce an F-center in LiF by different types of radiation has been determined by Morehead and Daniels[21] and is reported in Table 1.

Table 1. Energy (eV) required to produce an F-center in LiF (from ref. 21)

Radiation	Initial	after 10^6 rad	after 10^8 rad
2 MeV alpha particles	700	700	700
2 MeV electrons	140	140	700
1 MeV gamma photons	62	160	700
Thermal neutrons	65	100	700

3.3.2. Effect on the Glow Curve:

Morehead and Daniels[21] also determined the effect of different types of radiation on the glow curve areas for a given F-center concentration created by that radiation. The results are reported as in Table 2.

Table 2. Glow curve areas produced from F-center concentrations of 2×10^{18} cm^{-3}. (from ref. 21)

Radiation producing 2×10^{18} F-centers cm^{-3}	Area (in^2/mg LiF)
10^6 rad thermal neutrons	2500
10^6 rad betatron	2200
1.5×10^6 rad gamma photons	2000
10^7 rad alpha particles	4000

3.4. Li Isotopic Abundance:

As described in section 1, LiF is available in three different forms: TLD-100, containing 92.5% ^{7}Li and 7.5% ^{6}Li; TLD-600, containing 95.62% ^{6}Li and 4.38% ^{7}Li; and TLD-700, containing 99.99% ^{7}Li and 0.01% ^{6}Li.

3.4.1. Effect on Photon Response:

For ^{60}Co and Ra gamma rays, Kastner et al.[22] found the responses of TLD-700 to be very nearly the same. The ^{60}Co gamma-ray response for the EG and G dosimeters used in this research (see section 4.1 for description) was investigated and is reported in section 6.2.

3.4.2. Effect on Neutron Response:

Neutron induced thermoluminescent response in LiF is a secondary process resulting from ionizing radiations produced by neutron reactions on Li. Fluorine reactions are also possible, but should be identical for both TLD-600 and TLD-700. Since the cross sections for neutron reactions are energy dependent, it is necessary to consider the neutron response over energy ranges.

3.4.2.(a). Thermal Neutrons:

Inspection of the thermal neutron cross section tables[23] for ^{6}Li and ^{7}Li reveals a large (945 b) cross section for the $^{6}Li(n,\alpha)^{3}H$ reaction. The alpha particle is a highly ionizing particle, and the ^{3}H atom emits a highly ionizing beta particle, both of which can easily create traps in the LiF phosphor. Therefore the ^{6}LiF thermoluminescent response is large compared to the negligible ^{7}LiF response, because a thermal neutron reaction leading to trap production by ionizing radiation does not occur to a significant extent in ^{7}Li.

3.4.2(b). Fast Neutrons:

For neutrons up to 1.2 MeV in energy, the response of TLD-700 has been reported to be negligible compared to the TLD-600 response[22]. For the 14.7 MeV neutrons produced by the Cockcroft-Walton accelerator described in section 4.4, the total neutron cross sections for ^{6}Li and ^{7}Li are nearly the same.

The response characteristics of TLD-600 and TLD-700 for 14.7 MeV neutrons were investigated and are reported in section 6.3.

3.4.3. Mixed Radiation Field Studies:

In a mixed field of thermal neutrons and gamma rays, TLD-600 and TLD-700 can be irradiated simultaneously, and the response due to the individual components of the radiation field can be determined. The TLD-700 response can be taken as the response due to gamma rays alone, and since the TLD-600 responds to both thermal neutrons and gamma rays, the difference between the TLD-600 response and the TLD-700 response can be taken as the response due to thermal neutrons alone.

For discrimination between gamma rays, thermal neutrons, and fast neutrons up to 1.2 MeV, a series of three dosimeters has been used[1]. The first dosimeter was composed of TLD-700 and measured primarily the response due to gamma rays alone. The second dosimeter was composed of TLD-600 and measured the response due to thermal neutrons and gamma rays. The third dosimeter was composed of TLD-700 surrounded by ethyl alcohol. The fast neutrons collided with the hydrogen nuclei of the alcohol, thus projecting energetic protons into the LiF grains and giving rise to indirect fast-neutron response. This third dosimeter provided a measure of the response due to gamma rays and fast neutrons.

Oltman et al.[24] investigated the effect of neutron irradiation on the gamma-ray response of ^{7}LiF for both simultaneous

neutron irradiation and post-gamma neutron irradiation. Generally, they report a decrease of from 8% to 12% in the thermoluminescent response regardless of whether the neutron irradiation was carried out simultaneous with or following the gamma irradiation. The percentage drop is also reported to be independent of the total exposure and the energy of the neutron exposure up to 1 MeV. Neutron irradiation time was used as a relative measure of fluence in their data, but no indication of the response, if any, due to neutrons alone was given.

4. DESCRIPTION OF APPARATUS

4.1. DOSIMETERS:

Two types of LiF miniature dosimeters were used in this research. Model TL-22 dosimeters, containing TLD-600, and model TL-23 dosimeters, containing TLD-700, both manufactured by Harshaw Chemical Co. were supplied by Edgerton, Germeshausen, and Grier (EG and G). Each dosimeter contained about 10 mg of LiF phosphor sealed in a glass capillary 1.4 mm in diameter and 12 mm long. The tips of the dosimeter were color coded with blue (TL-22) and pink (TL-23) glass to insure against loss of identity.

The dosimeters were useful over a range of 10mR to 10^5R for gamma-photon irradiations, although they were nonlinear above 10^3R. Response was slightly energy dependent for photons, but the response had negligible temperature dependence at room temperature. Kaiseruddin[17] reported some dose-rate dependence at very high dose rates for the very similar TL-21 natural LiF dosimeter.

Response was reproducible to $\pm$3% above 1 R and to $\pm$20% at 10 mR. Each of the dosimeters was supposed to contain very nearly the same amount of phosphor, but to account for the very slight fluctuations in the phosphor weight, geometry of different ampules, varying grain sizes and sensitivities, dosimeters were preselected in a batch by the manufacturer such that the response values were supposed to be within $\pm$10% of the mean.

4.2. READER UNIT:

An EG and G model TL-3B Thermoluminescent Dosimeter Reader was used for dosimeter readout. The function of the reader unit was to position the dosimeter for readout, provide a heater current, detect the light emitted by means of a PM tube, convert the emitted light to an electrical signal, and provide a permanent chart record of the resulting glow curve. The reader was enclosed in a single aluminum cabinet 18 inches deep, 20 inches wide, and 13 inches high. The reader unit is shown in Fig. 3.

A block diagram of the circuitry of the reader unit is shown in Fig. 4. A regulated power supply fed the unit. When the READ push button was depressed, a heater current of 6.5 A was supplied to the read head adapter which held the dosimeter in the proper position. Light emitted from the dosimeter was reflected toward the PM tube. The signal from the PM tube was routed through the automatic ranging circuit to the pen servo-mechanism. The sensitivity of the PM tube was originally set to its maximum, which gave the lowest range on the recorder. When the light output increased beyond this range, the sensitivity of the PM tube was lowered by a factor of 10 by the automatic ranging circuit. The control logic sequenced these events so that readings from the lowest full scale range, 50mR, to the highest full scale range, 5 kR, were possible with a single depression of the READ button. Upon completion of the readout, the status indicator gave the full scale range of the recorder.

Fig. 3. EG and G model TL-3B thermoluminescent dosimeter reader unit.

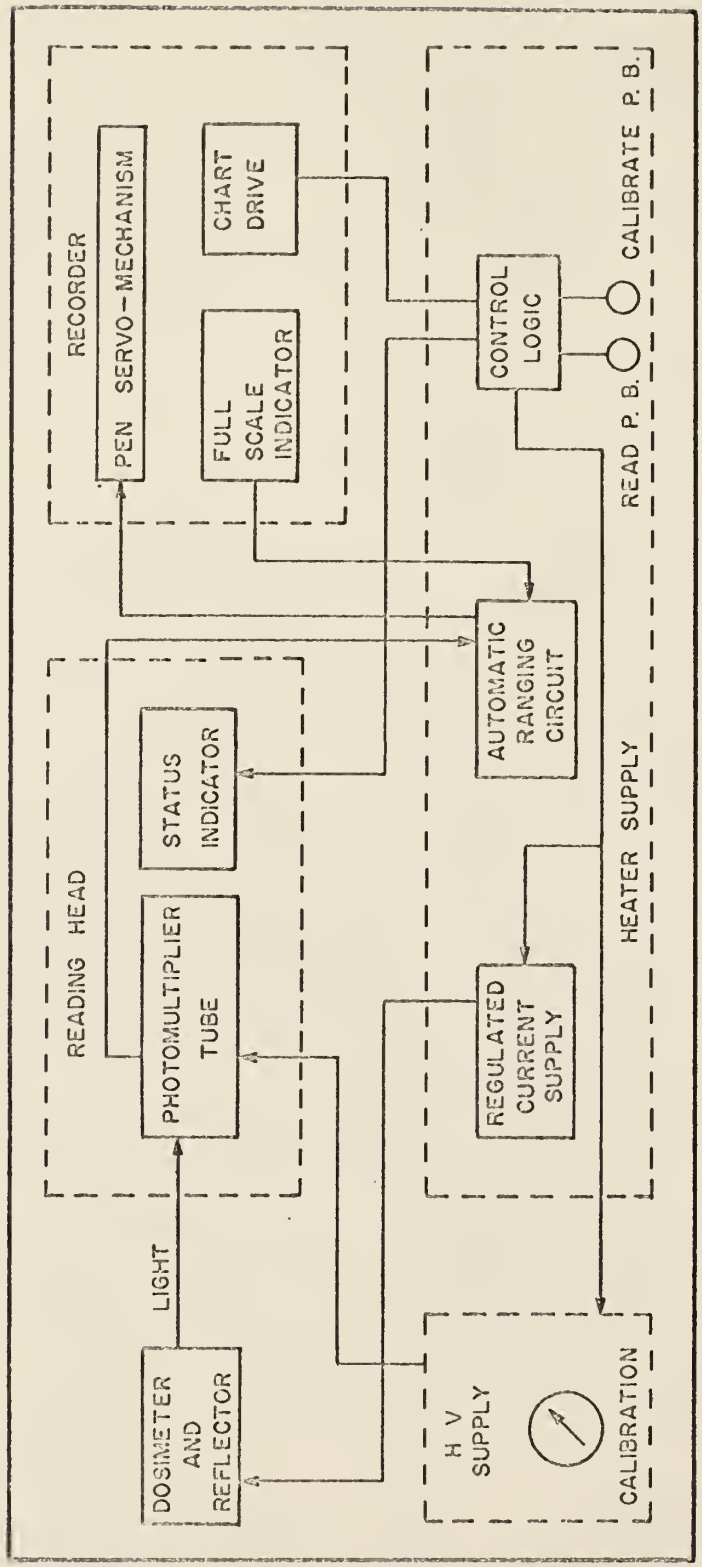

Fig. 4. Block diagram of reader unit circuitry.

A reference light was provided which enabled the system to be adjusted for accurate readings relative to a known reference. The reference light was constructed for use with the model TL-81 read head adapter. The reference light contained ^{14}C intimately mixed with thermoluminescent calcium fluoride. The beta radiation emitted from the ^{14}C caused the calcium fluoride to emit a glow which was equivalent to 340 mR. This value was determined by EG and G by exposing reference detectors to a ^{60}Co radiation dose measured by an NBS-calibrated ionization chamber, computing the average output of the detectors, and comparing it with the output of the reference light.

A typical chart record obtained with this reader unit is shown in Fig. 5. The heater current turned on when the recorder reached the short vertical line near the center of the chart and turned off at the end of the chart. The pen marking at the top of the chart shows a small "pip" each time a change of scale took place. Thus, knowing the lowest full scale range, the final full scale range could be ascertained by counting the number of "pips" on the chart, as well as by reading the status indicator.

The EG and G model TL-81B read head adapter shown in Fig. 6 was used to position and heat the dosimeters in the reader unit. The read head adapter was inserted in the front of the reader unit and enclosed the dosimeter in a light tight chamber. The read head adapter consisted of a heating coil and a shunt resistance which could be adjusted so that the current allowed

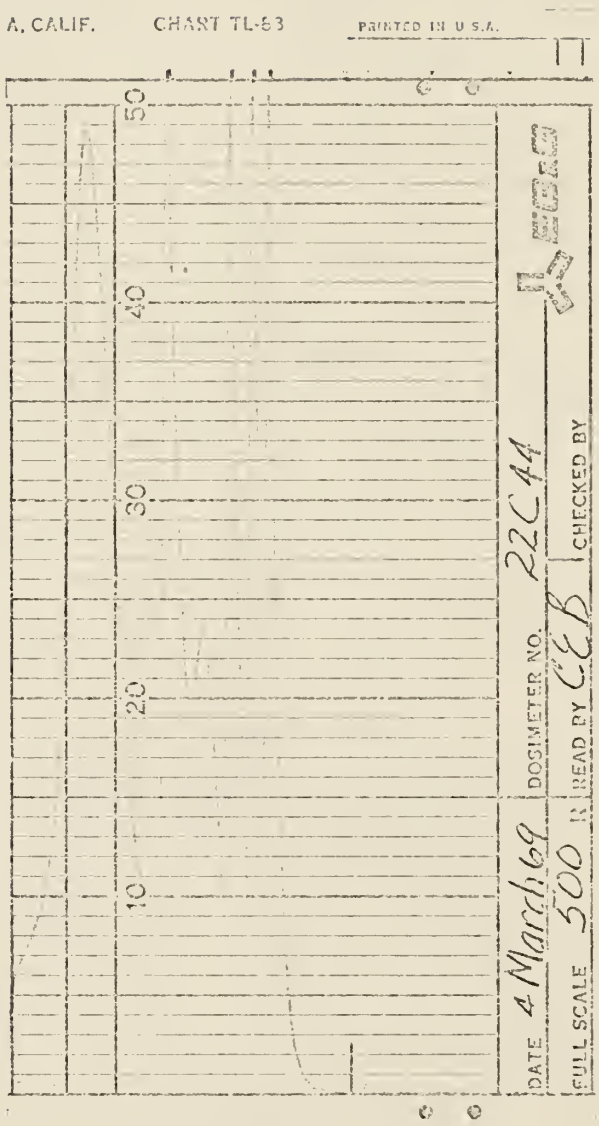

Fig. 5. Typical glow curve for gamma-irradiated dosimeter.

Fig. 6. EG and G read head adapter model TL-81B.

to flow through the heating coil resulted in the glow peak on the strip chart (Fig. 6) occuring near the middle of the 3 lines to the left of the chart.

Since the heating cycle was reproducible for each dosimeter, the peak height could be used as a measure of thermoluminescence, rather than the entire area under the glow curve.

4.3. GAMMACELL:

Gamma-photon irradiations were performed with a Gammacell 220 irradiation unit manufactured by Atomic Energy of Canada Ltd. The Gammacell was loaded with a 3,963 Ci ^{60}Co source on March 15, 1965. The ^{60}Co source consisted of 12 linear source elements equally spaced in a stainless steel rack to form a radioactive cylindrical shell, 8.75 inches measured between centers of opposing elements. Each linear element consisted of a welded stainless steel pencil filled with metallic cobalt. Internal dimensions of each pencil were 0.395 inch in diameter and 8 inches in length.

A motor driven drawer of the assembly consisted of a steel-encased lead cylinder 53.75 inches long and 6.5 inches in diameter. The drawer was centrally located in a surrounding radiation shield and was driven vertically through the center of the source. The drawer consisted of solid upper and lower sections and a hollow sample chamber. Material to be irradiated was placed in the sample chamber and then lowered to the irradiation position with the sample chamber at the center of

the source. The sample chamber was 8.125 inches in height and had an inside diameter of 6.0625 inches.

Control of the Gammacell was from a panel mounted at the side of the unit. The control panel included a drawer 'Up' button, a drawer 'Down' button, a digital timer with a range of 0 to 999 hours, and a timer 'In' switch which enabled the timer to be admitted into the control circuit when desired.

Correct dose rate at the time of irradiation was obtained from a graph of dose rates available at the Gammacell.

4.4. NEUTRON GENERATOR:

Neutron irradiations were performed with a Texas Nuclear Corp. Neutron Generator (Fig. 7). For production of 14.7 MeV neutrons, the generator uses the following reaction:

$$ {}^{2}_{1}H + {}^{3}_{1}H \rightarrow {}^{1}_{0}n + {}^{4}_{2}He + 17.6 \text{ MeV}. $$

Figure 8 shows a block diagram describing the function of the 3 basic components of the generator. Operation of the generator depends on the production, extraction and acceleration of deuterium ions.

Fig. 8. Basic components of the neutron generator.

Ion Source	Accelerating Tube	Target
Production, Extraction, Focusing of Positive Ions	Acceleration of Positive Ions	Production of Neutrons

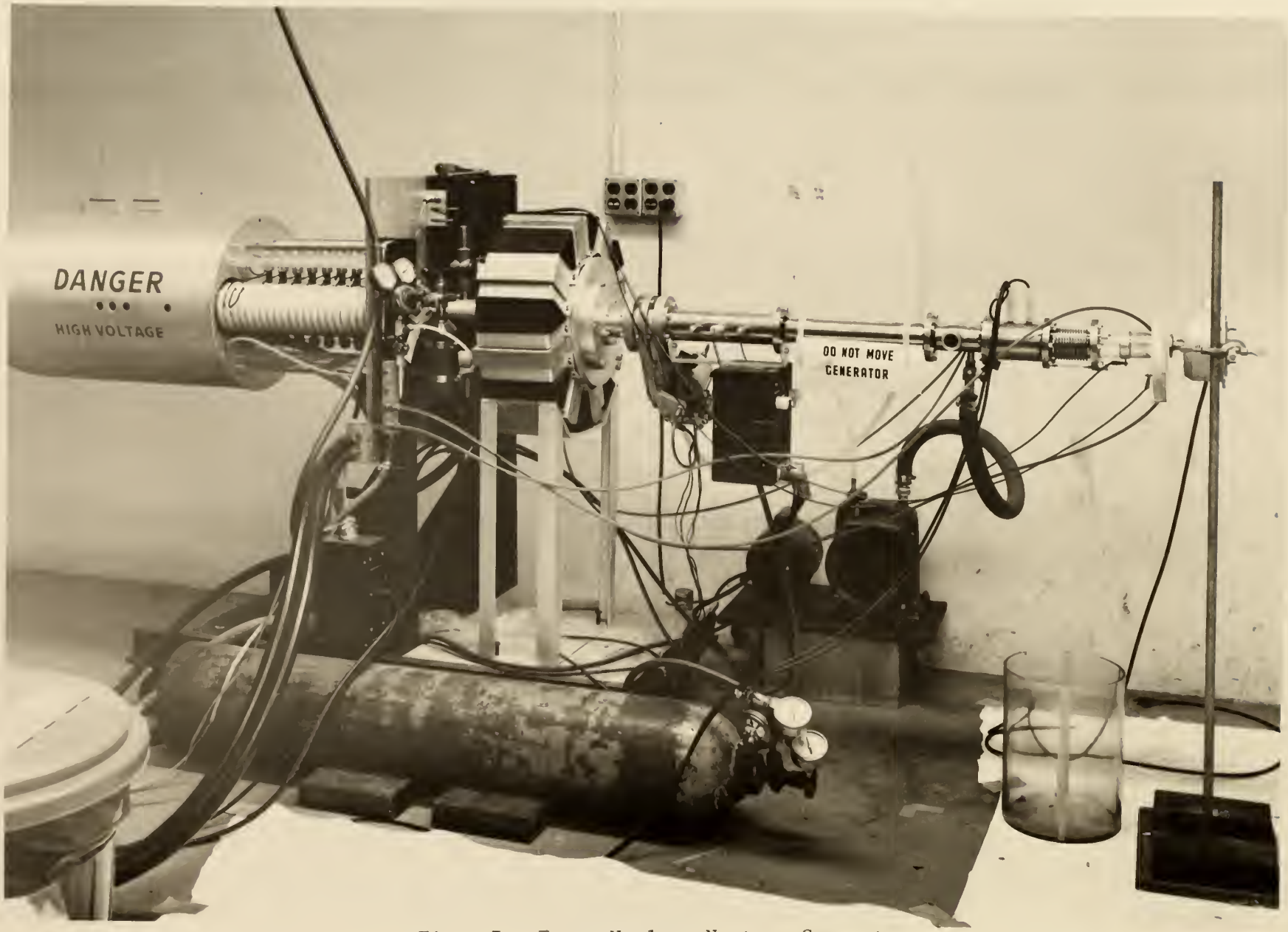

Fig. 7. Texas Nuclear Neutron Generator.

The major components of the neutron generator are shown schematically in Fig. 9. Positive ions created in a radio frequency type ion source were extracted by applying a potential across the ion source bottle. A quartz sleeve which surrounded the aluminum exit canal of the ion source bottle prevented surface recombinations of the ions. The quartz sleeve also served to focus the ion beam, as did the gap lens situated just beyond the exit canal. After passing the gap lens, the ions entered the field of the accelerating tube where they were accelerated through a potential of 150 kV. After leaving the accelerating tube, the ions drifted through a potential-free drift tube region until they fell on the tritium target, producing the desired reaction. The entire system was maintained in a vacuum to minimize scattering of the ion beam. An aluminum cap could be rotated for selection of one of the five available tritium targets. The neutron generator was operated from a remote console shown in Fig. 10.

The flux produced at the target was very nearly isotropic as shown in Table 3 which gives the neutron yield relative to forward emission[25]. Table 4 gives neutron energy as a function of emission angle[25].

Table 3. Neutron yield relative to forward emission.

Angle with Deuteron Beam	Neutron Yield (relative to 0°)
0°	1.00
60	.97
90	.94
120	.91
150	.88
180	.87

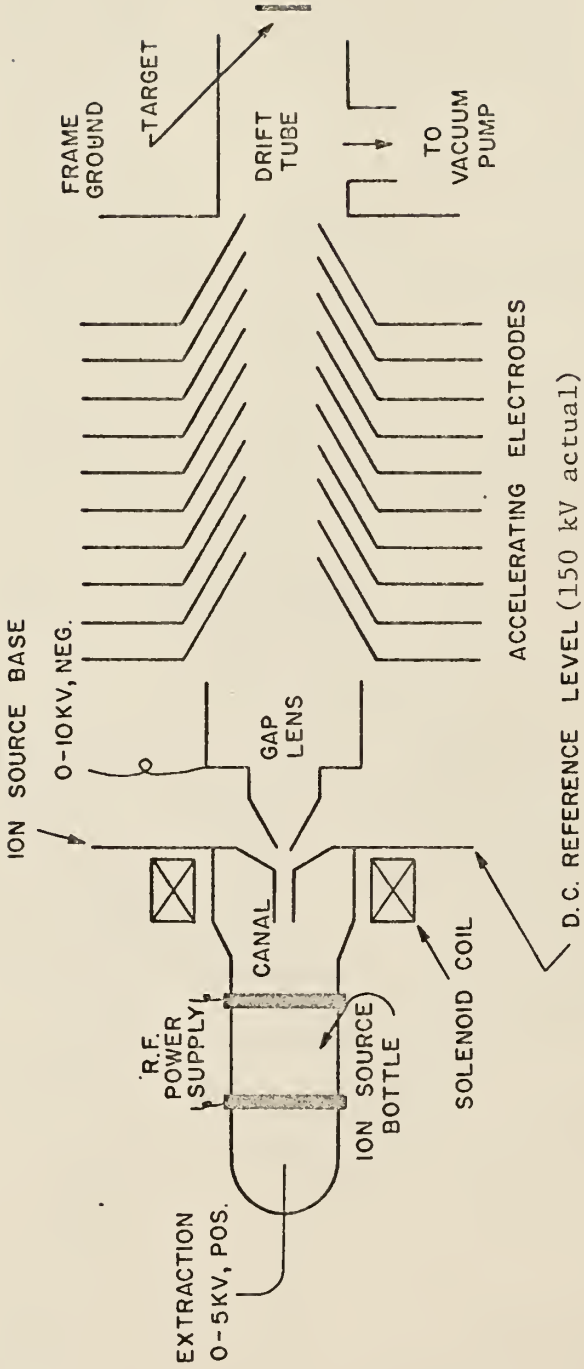

Fig. 9. Schematic of neutron generator. (Voltages shown are relative to ion source base.)

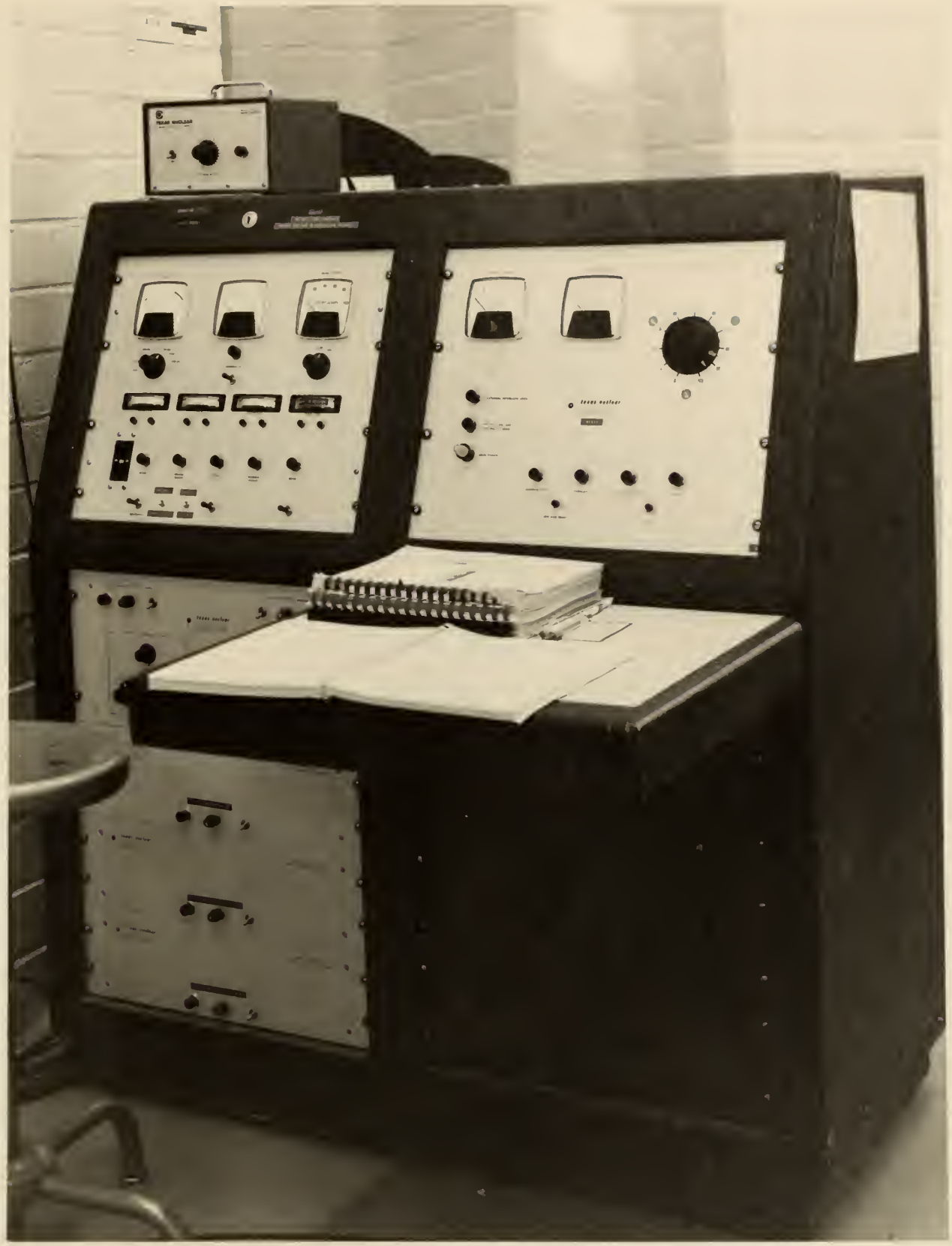

Fig. 10. Neutron generator remote console.

Table 4. Neutron energy as a function of emission angle. (E_d equals kinetic energy of deuterium ion)

Angle with Deuteron Beam	Neutron Energy E_d = 100 keV	E_d = 150 keV
0°	14.64 MeV	14.74 MeV
15	14.62	14.72
30	14.56	14.65
45	14.46	14.54
60	14.35	14.40
75	14.21	14.23
90	14.06	14.06
105	13.91	13.89
120	13.78	13.74
135	13.65	13.61
150	13.56	13.51
165	13.52	13.44
180	13.49	13.42

4.5. RADIATION DOSIMETER HOLDERS

4.5.1. Mounting in Gammacell:

A polyethylene disc about ½ inch thick, made to fit inside the sample chamber of the Gammacell was used in photon irradiations. Dosimeters were inserted vertically in the disc along the circumference of a 2 inch diameter circle concentric with the outer diameter. This insured that all dosimeters irradiated at the same time received the same amount of dose. The location of the disc within the sample chamber such that dosimeters located on the 2 inch diameter received the same dose as if they were located at the center of the chamber was determined from the iso-dose curves supplied by the manufacturer. For the 2 inch diameter, this height was 2.75 inch above the

base of the chamber. The Gammacell with dosimeter holder in place is shown in Fig. 11.

4.5.2. Mounting Near the Neutron Generator Target:

For neutron irradiation, an irradiation package consisting of polyethylene-enclosed dosimeters and an activation foil (see section 4.6) was used. The package was attached to a motorized assembly which rotated the dosimeters and activation foil about an axis perpendicular to the center of the accelerator target. The irradiation package was placed as near the accelerator target as possible with the foil between the target and the dosimeters. The irradiation package is shown in Fig. 12.

The best configuration for packaging of the dosimeters, was determined and is described in section 5.3.

4.6. ACTIVATION FOILS:

Sodium-24, produced from the $^{27}Al(n,\alpha)^{24}Na$ was the radioisotope chosen for use with the sum-peak method. The decay scheme of ^{24}Na is shown in Fig. 13.

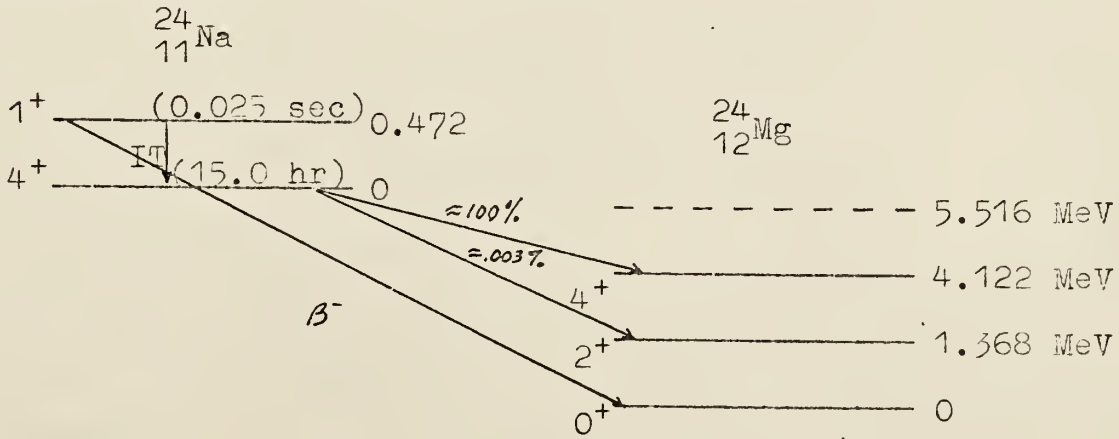

Fig. 13. Decay scheme of ^{24}Na.

Fig. 11. Gammacell with dosimeter holder in place.

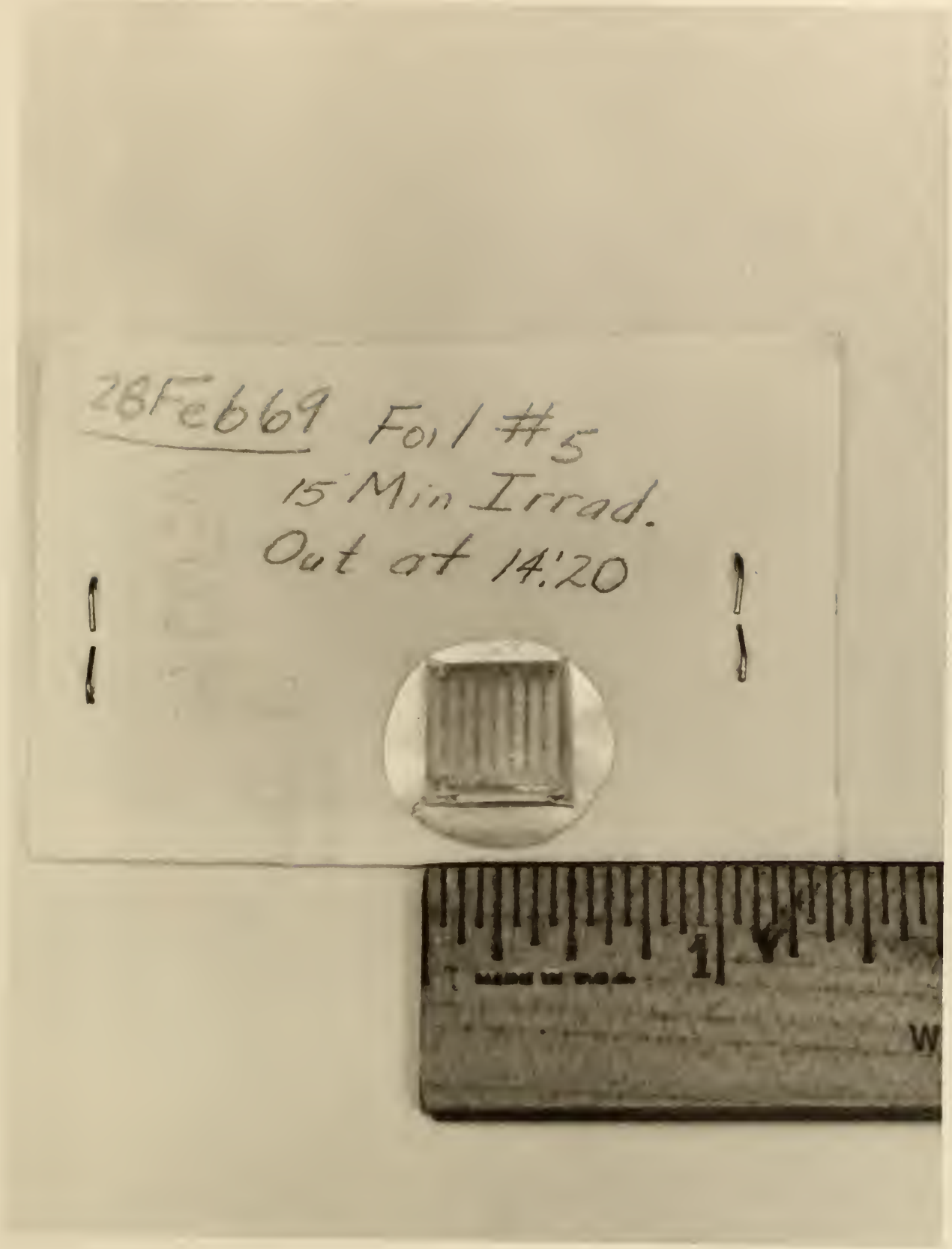

Fig. 12. Neutron irradiation package.

^{24}Na decays to ^{24}Mg which emits the required coincident gamma rays which are well separated in energy. The half life is fifteen hours. The ^{28}Al formed by the (n,γ) reaction and the ^{27}Mg formed by the (n,p) reaction have relatively short half lives of 2.3 and 9.5 minutes respectively. Therefore, within about two hours after irradiation, essentially only the desired ^{24}Na was present.

An additional advantage of the use of activated aluminum was the ready availability of aluminum in very pure thin foils. Commercial aluminum foil was used to make activation foils about 3/4 inch in diameter weighing approximately .0155 g.

The cross section for the $^{27}Al(n,\alpha)^{24}Na$ reaction was determined from the values tabulated in Table 5 which were taken from BNL 325[26]. The values were averaged, and the standard deviation of the average was determined by propagation of error. This resulted in a cross section of 115.3 ± 2.8 mb.

Table 5. Cross section tabulation for $^{27}Al(n,\alpha)^{24}Na$ reaction.

Author	Date	Energy	Cross Section
Kern	1959	14.7 MeV	113 ± 14 mb
Yasumi	1957	14.7	120 ± 15
Mani	1960	14.75	111 ± 3
Strohal	1962	14.6	115 ± 2
Jeronymo	1963	14.7	110 ± 10
Gabbard	1962	14.7	115 ± 10

Table 5. Cross section tabulation for $^{27}Al(n,\alpha)^{24}Na$ reaction. (continued)

Author	Date	Energy	Cross Section
Poularikas	1959	14.8 MeV	114 ± 7 mb
Butler	1962	14.68	115 ± 5
Bermann	1961	14.7	120 ± 5
Bayhirst	1961	14.68	119.5 ± 6

4.7. SPECTROMETER SYSTEM:

The spectrometer system used to count the activation foils was a Harshaw Chemical Co. NaI(Tl) solid scintillation detector with an attached RCA photomultiplier tube. A Technical Measurements Corp. (TMC) preamplifier was used with this integral line assembly. The detector assembly was shielded by a cavity of 4 inch lead bricks walls lined with a 20 mil layer of cadmium and a 20 mil layer of copper. A TMC 4096 multiparameter analyzer operating in the pulse height mode was used with the detector system. Figure 14 shows a block diagram of the detection instrumentation. A typical ^{24}Na spectrum obtained with this spectrometer system is shown in Fig. 15.

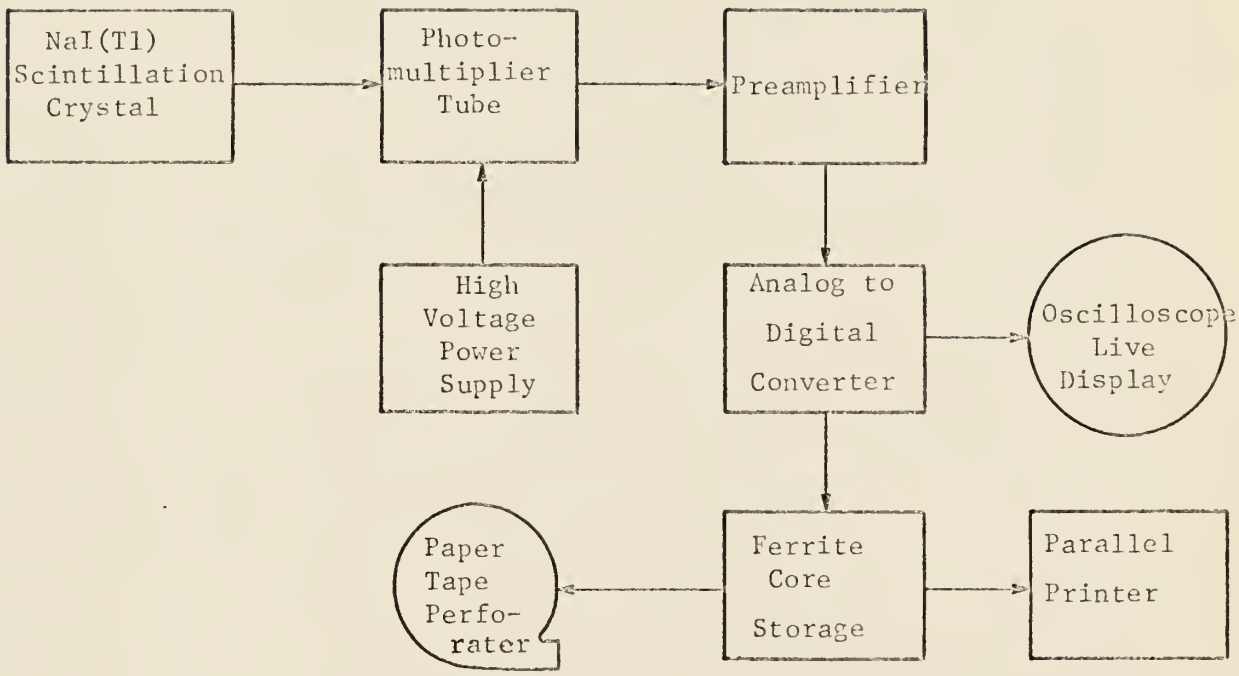

Fig. 14. Block diagram of detection instrumentation.

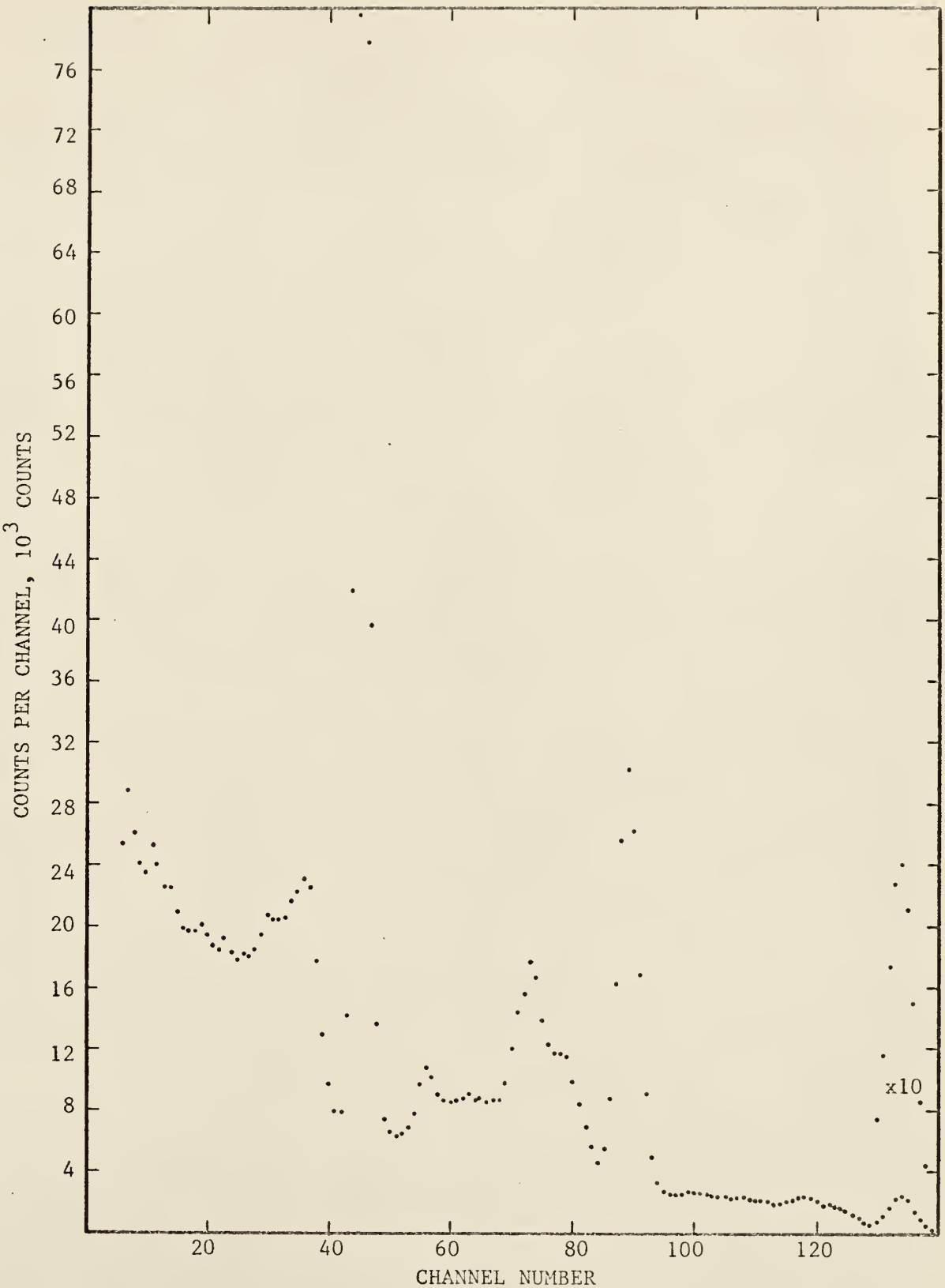

Fig. 15. Typical ^{24}Na-decay spectrum.

5. PRELIMINARY EXPERIMENTAL PROCEDURES AND FINDINGS

5.1. FADING STUDIES

5.1.1. Procedure:

Fading effects in LiF thermoluminescent dosimeters have been described in section 3.2.1. There were inconsistencies reported in the literature concerning the proper way of removing the fading effects. From the typical glow curve of Fig. 2, it was seen that the distinct low temperature peak appeared at 105°C. Therefore the annealing procedure of Dean and Larkins[20] appeared to be more logical since annealing at 110°C for 7 minutes should be effective in removing this peak. This postirradiation annealing technique was investigated for comparison with a procedure of no postirradiation annealing.

One hundred TL-22 dosimeters and one hundred TL-23 dosimeters were irradiated to about 200 R by a 4 sec irradiation in the Gammacell. Fifty of the TL-22's and fifty of the TL-23's were subsequently annealed at 110°C for 7 minutes. For all annealing procedures the dosimeters were placed vertically in a 1 inch thick graphite block drilled with small holes approximately 5 mm deep spaced about ¼ inch apart and fed into the furnace. The unannealed and partially annealed dosimeters were then read out in groups of ten at five different times over a period of 72 hours. For each group of ten dosimeters, a mean response and the standard deviation of the mean response were calculated.

5.1.2. Results:

The results of the fading study for ^{6}LiF are presented in Figs. 16 and 17. The results of the fading study for ^{7}LiF are presented in Figs. 18 and 19.

For ^{7}LiF, Figs. 18 and 19 show that the partial annealing process had little effect on the thermoluminescent response or the standard deviation of the response up to 2 days after the irradiation. However, 3 days after the irradiation, fading did appear in the unannealed dosimeters.

For ^{6}LiF, Fig. 16 shows that the response of the unannealed dosimeters was very inconsistent over the 72 hour period of readout. The partial annealing process had an unusual effect on the ^{6}LiF response. Figure 17 shows that the response was considerably lower than the average during the first few hours after irradiation but was quite consistent after approximately 24 hours.

5.1.3. Conclusions:

For control of later experiments involving both the ^{6}LiF and ^{7}LiF thermoluminescent response, it was necessary to be consistent in postirradiation annealing and readout procedure. The inconsistency of unannealed ^{6}LiF dosimeter response ruled out the non-annealing process. If the partial annealing process were to be used, however, readout of the ^{6}LiF dosimeter would be inconsistent unless readout was performed at least 24 hours after irradiation. Therefore the following procedure was adopted:

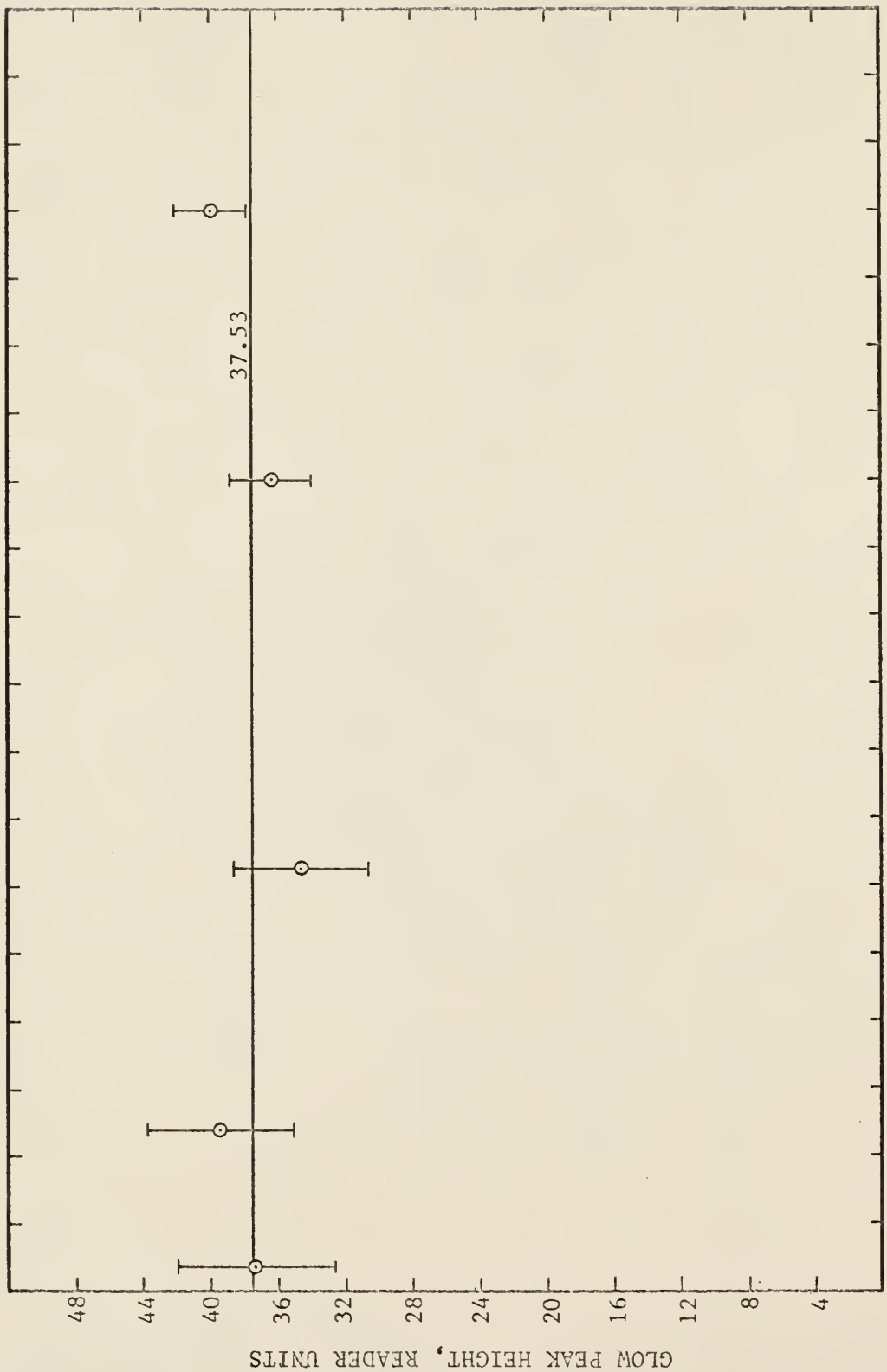

Fig. 16. Dosimeter response vs. fading time for unannealed E G and G model TL-22 dosimeters. (^{6}LiF)

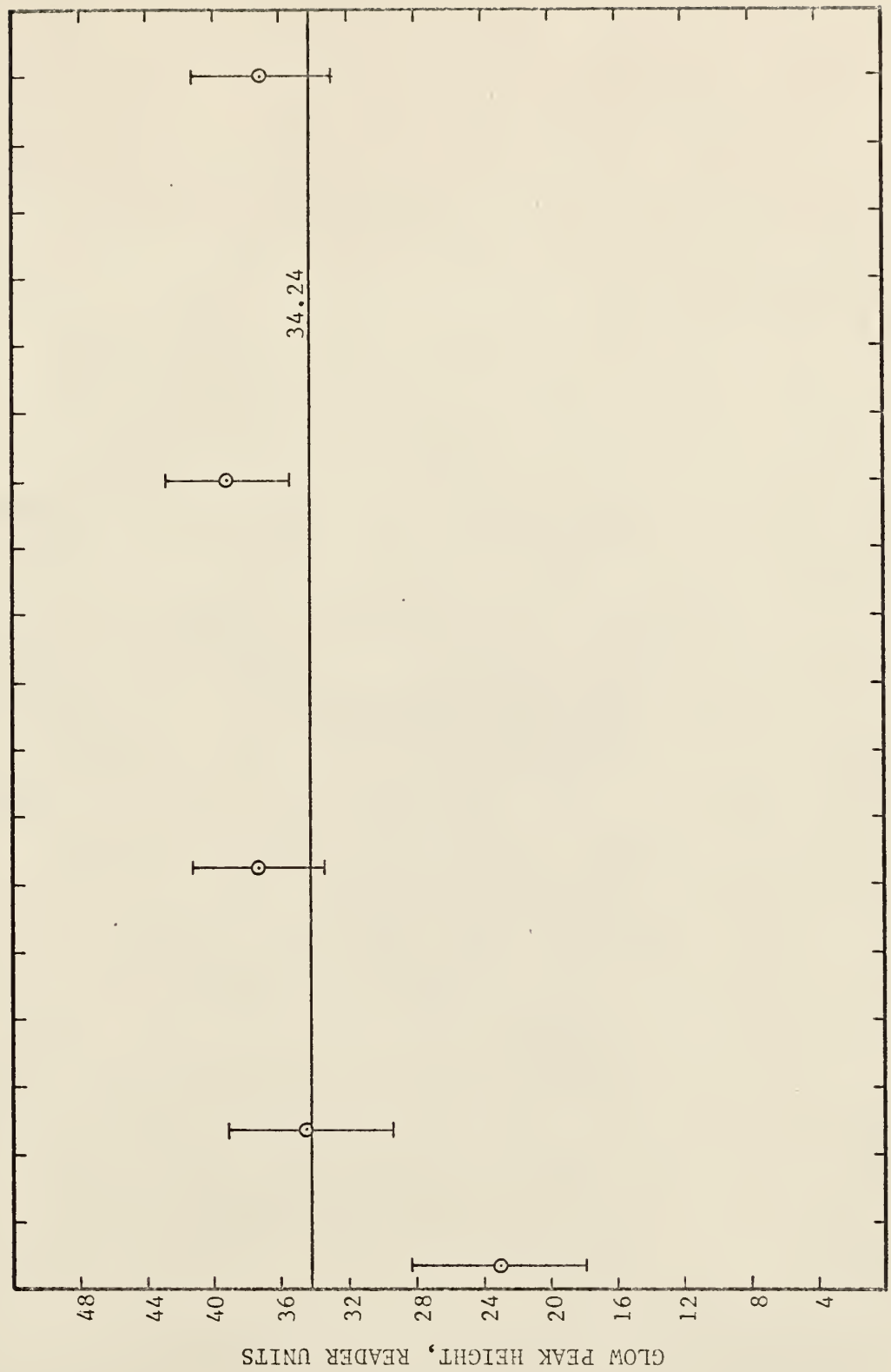

Fig. 17. Dosimeter response vs. fading time for partially annealed E G and G model TL-22 dosimeters. (^{6}LiF)

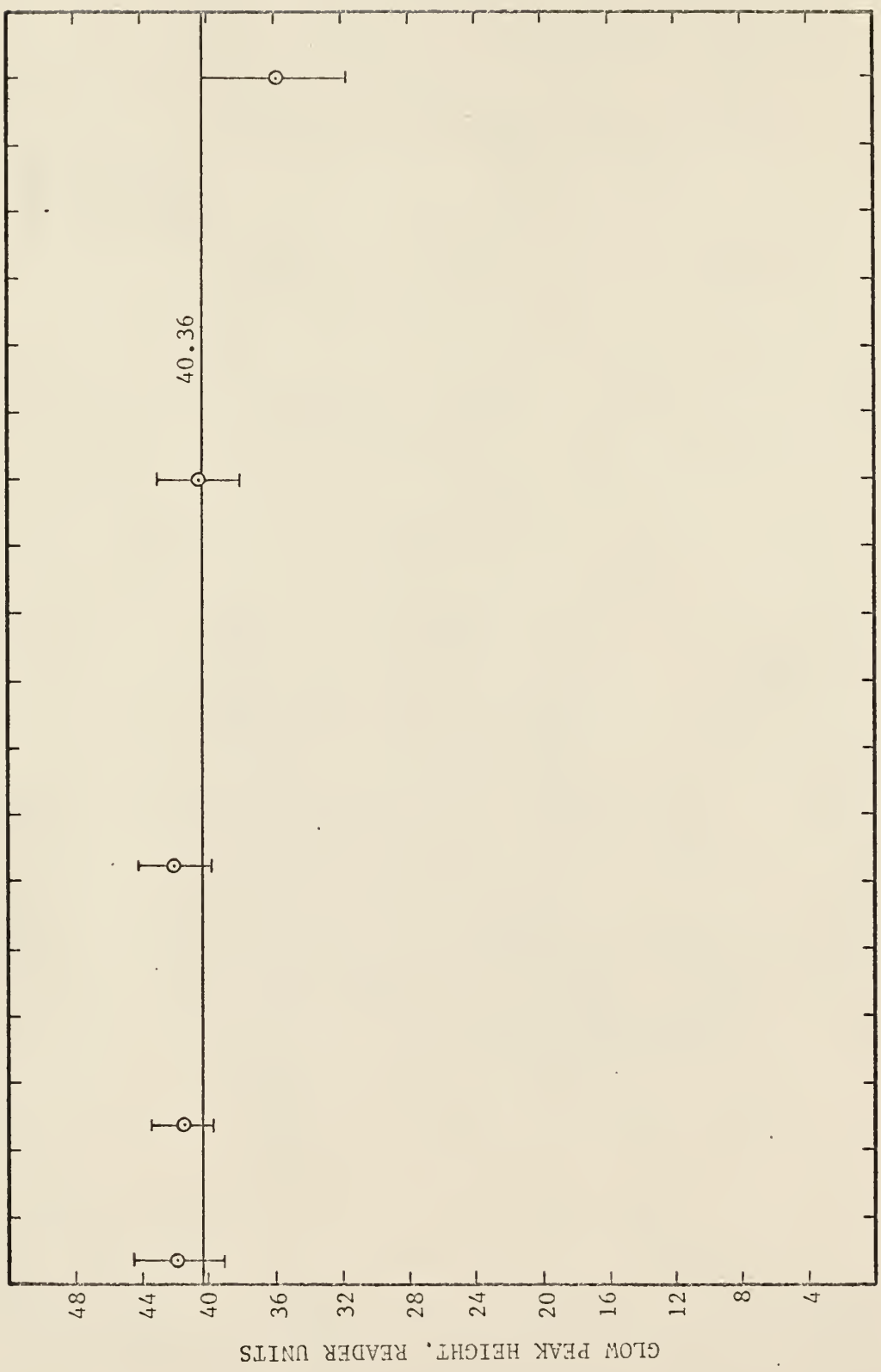

Fig. 18. Dosimeter response vs. fading time for unannealed E G and G model TL-23 dosimeters. (^{7}LiF)

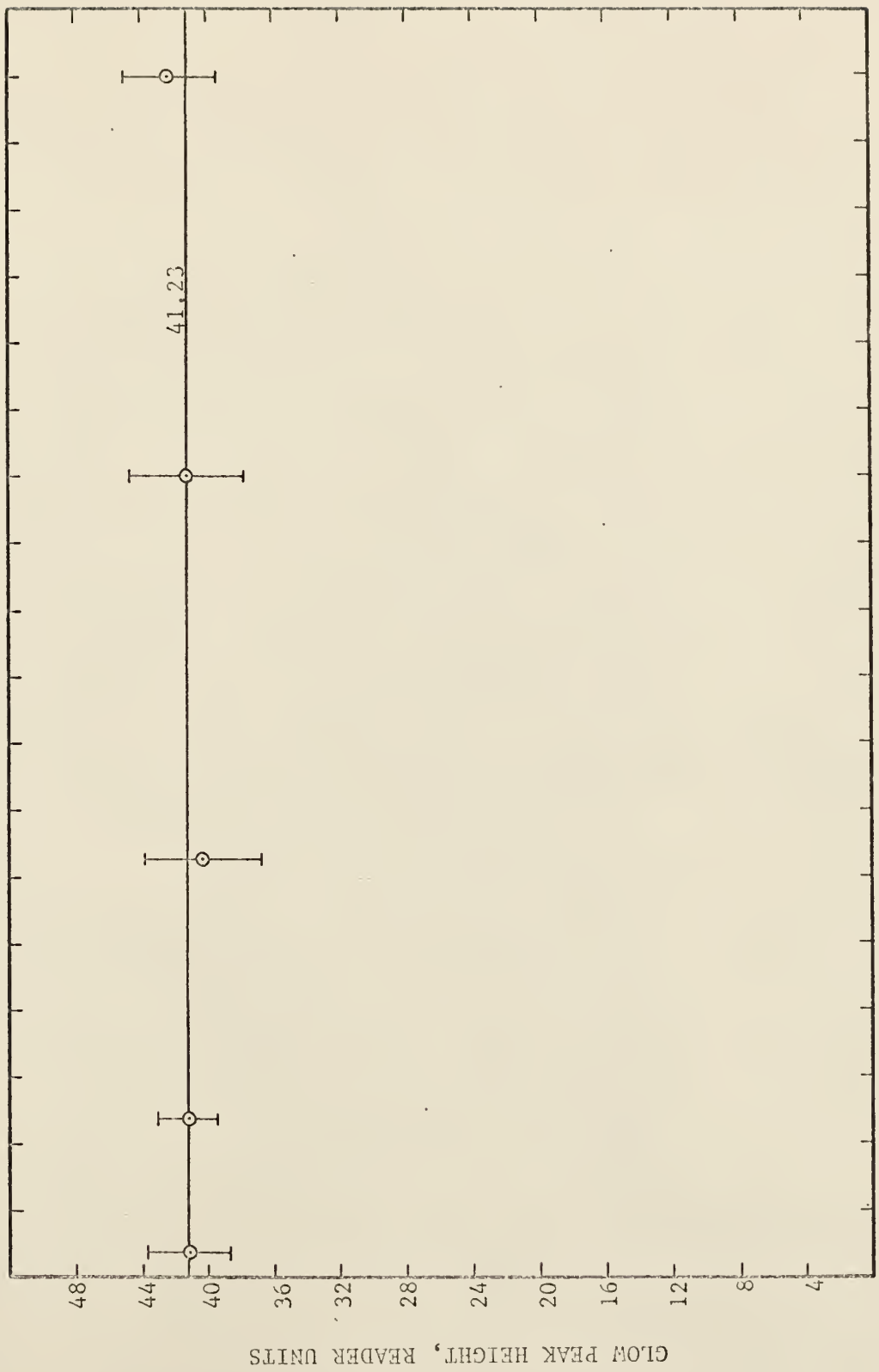

Fig. 19. Dosimeter response vs. fading time for partially annealed E G and G model TL-23 dosimeters. (^{7}LiF)

a) all dosimeters were partially annealed after irradiation for 7 minutes at 110°C, and

b) all dosimeters were read out at least 24 hours after irradiation.

5.2. ESTIMATION OF THE GAMMA-RAY CONTAMINATION ON THE NEUTRON GENERATOR

5.2.1. Basis of Contamination Determination:

For neutron irradiation, dosimeters were placed behind an activation foil as described in section 4.5.2. The flux of neutrons at the target was nearly isotropic (see Table 3) and activity was therefore also induced in all directions around the target in the accelerator components, primarily in the aluminum cap which held the 5 tritium targets. This activity induced in the activation foil and the aluminum cap could cause an additional response due to gamma rays in the neutron irradiated dosimeters. Since the activation foil and accelerator cap were both aluminum, the reactions of concern were the $^{27}Al(n,\gamma)^{28}Al$ reaction, the $^{27}Al(n,p)^{27}Mg$ reaction, and the $^{27}Al(n,\alpha)^{24}Na$ reaction. The activation cross sections of these reactions are approximately 215, 80, and 115 millibarn, respectively. The half lives of the products are 2.3 min., 9.5 min., and 15 hr., respectively.

As described in section 2.4.3, the activity of isotope B caused by the neutron activation of isotope A is

$$N_B \lambda_B = \Phi \sigma N_A (1 - e^{-\lambda_B t}). \qquad (2.4.3\text{-}1)$$

After removal from the neutron flux, the activity is

$$N_B \lambda_B = \Phi\sigma N_A(1 - e^{-\lambda_B t}) e^{-\lambda_B \bar{t}} . \qquad (2.4.3\text{-}2)$$

For each of the three reactions, the flux, Φ, and N_A, the atoms of material A were constant. Therefore, during irradiation, the activity of each of the activation products, B_i, was proportional to the product of the activation cross section and the term $(1 - e^{-\lambda_{B_i} t})$.

$$N_{B_i}\lambda_{B_i} \quad \alpha \quad \sigma_i(1 - e^{-\lambda_{B_i} t}) \qquad (5.2\text{-}1)$$

After irradiation, the activity of each of the activation products is proportional to the product of the activation cross section, the term $(1 - e^{-\lambda_{B_i} t})$ and the term $(e^{-\lambda_{B_i} \bar{t}})$.

$$N_{B_i}\lambda_{B_i} \quad \alpha \; \sigma_i(1 - e^{-\lambda_{B_i} t})e^{-\lambda_{B_i} \bar{t}} \qquad (5.2\text{-}2)$$

Using equation (5.2-1), the buildup of each of the three activation products was calculated over a 25 minute irradiation period. Using equation (5.2-2), the decay of each of these products was calculated over a 60 minute period following the 25 minute irradiation. The buildup and decay of each of the products is shown in Fig. 20.

The total activity of each of the activation products induced during an irradiation time, t, was proportional to the area from 0 to t under the three time functions defined by equation (5.2-1). After irradiation, the total activity of the activation products during a decay time from t to $\bar{t}$ was proportional to the area from t to $\bar{t}$ under the three time functions

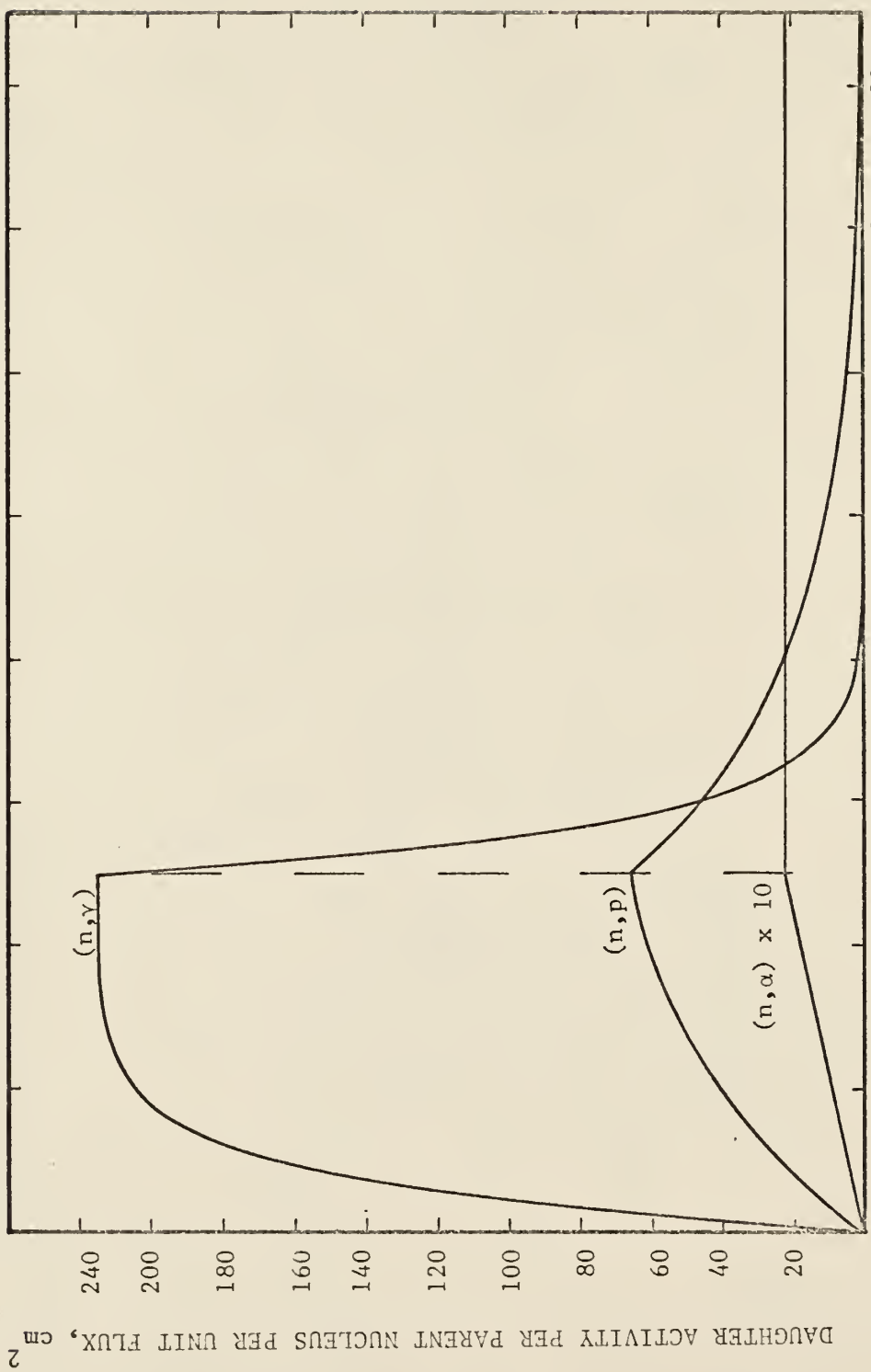

Fig. 20. Buildup and decay of activation products of ^{27}Al.

defined by equation (5.2-2). By trapezoidal integration of the functions defined by equation (5.2-1) and equation (5.2-2), the ratio of the total activity from 0 to t to the total activity from t to $\bar{t}$ could be obtained. This ratio was the same as the ratio of the dosimeter response due to gamma rays from 0 to t to the dosimeter response due to gamma rays from t to $\bar{t}$. The total activity during the irradiation period and the dosimeter response due to this total activity could not be directly measured. However, by placing a package of unirradiated dosimeters in position with the activation foil and accelerator components immediately following a neutron irradiation, the dosimeter response due to induced activity during a decay period could be determined. This response could then be related to the response due to activity induced during the irradiation period by multiplication by the ratio of total activities determined by trapezoidal integration.

5.2.2. Procedure and Results: .

A package of ten dosimeters, five TL-22's and five TL-23's was irradiated 25 minutes on the neutron generator. A second identical package of ten dosimeters was positioned immediately after the irradiation in the place previously occupied by the first package. The second package of dosimeters was allowed to absorb gamma-ray dose from the activation foil and the aluminum cap for a period of 60 minutes. All dosimeters were then annealed for 7 minutes at 110°C and read out after 24 hours.

From the first package, the response of the neutron irradiated TL-22's was 72.0 ± 17.8 reader units (R.U.). The response of the neutron irradiated TL-23's was 63.4 ± 7.8 R.U. The response of the gamma irradiated TL-22's from the second package was 248 ± 15.6 mR.U. The response of the gamma irradiated TL-23's was 296.2 ± 60.4 mR.U.

The results of the trapezoidal integration from Fig. 20 are presented in Table 6. Also presented are similar results for a 60-minute irradiation.

Table 6. Trapezoidal integration of equations (5.2-1) and (5.2-2). (All areas have units of cm^2.)

Reaction	A_1, area 0 to 25 min	A_2, area 25 to 85 min	A_3, area 0 to 60 min	A_4, area 60 to 120 min
(n, γ)	4656.42	718.56	12180.95	718.94
(n,p)	1080.95	908.48	3716.61	1069.76
(n, α)	28.69	134.15	163.79	317.68
Total	5765.06	1761.19	16061.35	2106.39

Multiplication of the gamma-ray responses reported above by the ratio of total A_1/A_2 gave an estimate of the response due to gamma activity during the irradiation. Thus the response due to gamma-ray activity during a 25 minute irradiation was found to be 811.8 mR.U. for TL-22 and 969.6 mR.U. for TL-23. These values represent 1.13% of the TL-22 neutron response and 1.53% of the TL-23 neutron response for a 25 minute irradiation.

If a 60 minute irradiation were carried out at the same flux level, the response due to gamma rays during the irradiation would be increased by a factor of A_3/A_1. The neutron response would be increased approximately by a factor of 60/25. In this case, the gamma-ray response would represent 1.31% and 1.77% of the neutron response for TL-22 and TL-23, respectively.

For all the various time durations of neutron irradiation used in the determination of the neutron calibration curves, the gamma-ray response represented only between 1% and 2% of the neutron response, and was therefore neglected.

5.3. DETERMINATION OF BEST DOSIMETER PACKAGE CONFIGURATION:

The tritium targets of the accelerator were approximately 1 inch in diameter, and the activation foils were approximately 3/4 inch in diameter. Ten dosimeters placed side by side in a small polyethylene cover resulted in a dosimeter package just under 3/4 inch across, so that the activation foil just covered the package. However, irradiation in this configuration generally resulted in 1 or 2 dosimeter responses which were extremely low. These low responses generally occurred for the dosimeters at the edges of the irradiation package.

To improve the standard deviation of the response of neutron irradiated dosimeters, a method to eliminate the extremely low responses was sought. Therefore, instead of packaging the dosimeters ten across, irradiation of dosimeters placed eight across, several packages in depth, was investigated. The results are presented in Table 7.

Table 7. Results of multiple packaging of dosimeters for neutron irradiation.

Package No.	Average Response
1 (nearest the target)	20.3 ± 2.3
2	19.1 ± 1.5
3	14.5 ± 1.8

The composite average of the response from the first two packages was 19.7 ± 2.0. The response values from the third package were much lower than those of packages 1 and 2. Based on these data, it was concluded that geometric and material attenuation were such as to limit the number of packages to two in depth.

6. DETERMINATION OF CALIBRATION CURVES

6.1. NECESSITY OF CALIBRATION CURVES:

Since the peak height measured on the glow curve from the EG and G reader unit gave the dosimeter response in relative units, it was necessary to obtain a calibration for converting response to dose or response to neutron fluence. Over the range 0 to 10^3 R, the response was supposed to be linear with respect to the dose. Therefore, a calibration factor, k, could be obtained for use over this range. In the range 10^3 to 10^5 R, the response was supposed to be reproducible but non-linear with respect to the dose. Therefore, a full experimental calibration curve was required over this range.

6.2. GAMMA-RAY CALIBRATION CURVE

6.2.1. Linear Calibration Function:

The dose rate in the Gammacell at the time of the calibration was 55.54 R/sec. The timer on the Gammacell allowed irradiation for any length of pre-set time. However, the timer did not start counting until the drawer of the assembly was in its lowest position. The drawer did not move upward until the end of the pre-set time. Therefore, the dosimeters absorbed a considerable amount of dose during the up and down travel of the drawer. This additional dose was a constant irrespective of the pre-set irradiation time.

In order to determine the additional dose absorbed by the dosimeters during the travel time, the following mathematical

model was used. If the dose rate in response units was represented by $\dot{R}$, the dose due to the constant additional dose by R_o, and the pre-set irradiation time by t, then the total response of the dosimeter, R, could be given by

$$R = R_o + \dot{R}t. \qquad (6.2.1\text{-}1)$$

The parameters R_o and $\dot{R}$ could be obtained by a least-squares analysis of the experimental response values in the range 0 to 10^3 R. Over this linear range, the calibration factor, k, having units of R per reader unit could then be obtained by dividing the known dose rate, $\dot{D}$, by the dose rate in response units, $\dot{R}$. The dose absorbed during the travel time was then calculated as the product of k and R_o. The total dose was then given by

$$D = D_o + \dot{D}t \qquad (6.2.1\text{-}2)$$

6.2.2. Experimental Procedure:

To determine the calibration curve, groups of twenty dosimeters, ten TL-22's and ten TL-23's, were irradiated at one time for pre-determined time periods set on the Gammacell timer. All dosimeter had been annealed for 1 hour at 400°C before irradiation. Following irradiation, the dosimeters were partially annealed at 110°C for 7 minutes. Dosimeters were read out 24 hours after the partial annealing.

6.2.3. Analysis of Data and Results:

Ten response values were available for analysis for each type dosimeter at each time setting. To limit the effects of

error in dosimeter response, the extreme values of response were eliminated at each data point. Thus, eight response values were used to determine the mean response and the standard deviation of the mean response at each point.

Using the response data for irradiation times of 0, 2, 6, and 12 seconds (i.e., the irradiation times resulting in a dose of less than 10^3 R), the values of $\dot{R}$ and R_o for each type dosimeter were calculated by a least squares analysis using equation (6.2.1-1). The fit was obtained using the eight individual response values at each time setting rather than the mean response at each time setting.

For the TL-22 dosimeters, $\dot{R}$ was calculated to be 4.52 $\pm$ .15 R.U./sec, and R_o was calculated to be 15.229 R.U. Therefore, k was calculated to be 12.288 R/R.U., and D_o was found to be 187.13 R. The total dose for each time setting was calculated by equation (6.2.1-2).

For the TL-23 dosimeters, $\dot{R}$ was calculated to be 5.539 $\pm$ .241 R.U./sec, and R_o was calculated to be 17.167 R.U. Therefore, k was calculated to be 10.027 R/R.U., and D_o was found to be 172.13 R. The total dose for each time setting was calculated by equation (6.2.1-2).

Theoretically, the dose calculated by equation (6.2.1-2) at each time setting should have been the same regardless of the type dosimeter used to calculate D. Because of the difference in the calculated values of D_o for each dosimeter type, there was a discrepancy of 15 R in the dose at each time setting. To

resolve this conflict, the experimental value of R_o (i.e., the response of each dosimeter type for a zero time irradiation) was used to calculate D_o. This resulted in values of D_o of 178.17 R and 176.17 R for TL-22 and TL-23 respectively. These values of D_o were then used to calculate a corrected dose at each irradiation time. This procedure reduced the discrepancy from 15 R to 2 R.

The results of the gamma ray calibration are presented in Table 8. The corrected dose values from Table 8 were plotted in Figs. 21 and 22 against the total response to obtain the calibration curves. Since the calibration was linear over the range 0 to 10^3 R, points were connected by a line with slope equal to the calibration factor, k. Above 10^3 R, the calibration line was drawn through the experimental points since the response was reproducible but not linear.

By comparison of Figs. 21 and 22, it was observed that the responses of TL-22 and TL-23 dosimeters to gamma dose were slightly different. Throughout the dose range investigated, the TL-23 response was about 20% higher than the TL-22 response.

6.3. NEUTRON CALIBRATION CURVE

6.3.1. General Considerations:

The neutron calibration was inherently more difficult than the gamma calibration. The dose rate in the Gammacell was known from prior calibration, but the dose rate of the neutron generator was not well known, nor was it constant. The dose

Table 8. Data and results for the gamma calibration curves.

S. No.	Irrad. time, sec.	Estimated dose*, R	Total Response, reader units	Corrected dose, R
22-1	0	0	14.50 ± 1.89	178.17
22-2	2	111.08	26.54 ± 3.27	289.25
22-3	6	333.24	40.63 ± 3.39	511.41
22-4	12	666.48	70.25 ± 5.09	844.65
22-5	24	1332.96	144.63 ± 6.55	1511.13
22-6	40	2221.6	269.13 ± 12.05	2399.77
22-7	60	3332.4	384.38 ± 31.44	3510.57
22-8	80	4443.2	566.25 ± 38.98	4621.37
22-9	100	5554.0	798.75 ± 117.65	5732.17
23-1	0	0	17.57 ± .45	176.17
23-2	2	111.08	33.63 ± 1.37	287.25
23-3	6	333.24	41.84 ± 2.27	509.41
23-4	12	666.48	88.38 ± 3.72	842.65
23-5	24	1332.96	177.13 ± 8.06	1509.13
23-6	40	2221.6	306.63 ± 14.63	2397.77
23-7	60	3332.4	512.13 ± 14.11	3509.57
23-8	80	4443.2	683.75 ± 40.33	4619.33
23-9	100	5554.0	906.11 ± 82.91	5730.17

*Estimated dose = (Dose rate in Gammacell x Duration of irradiation)

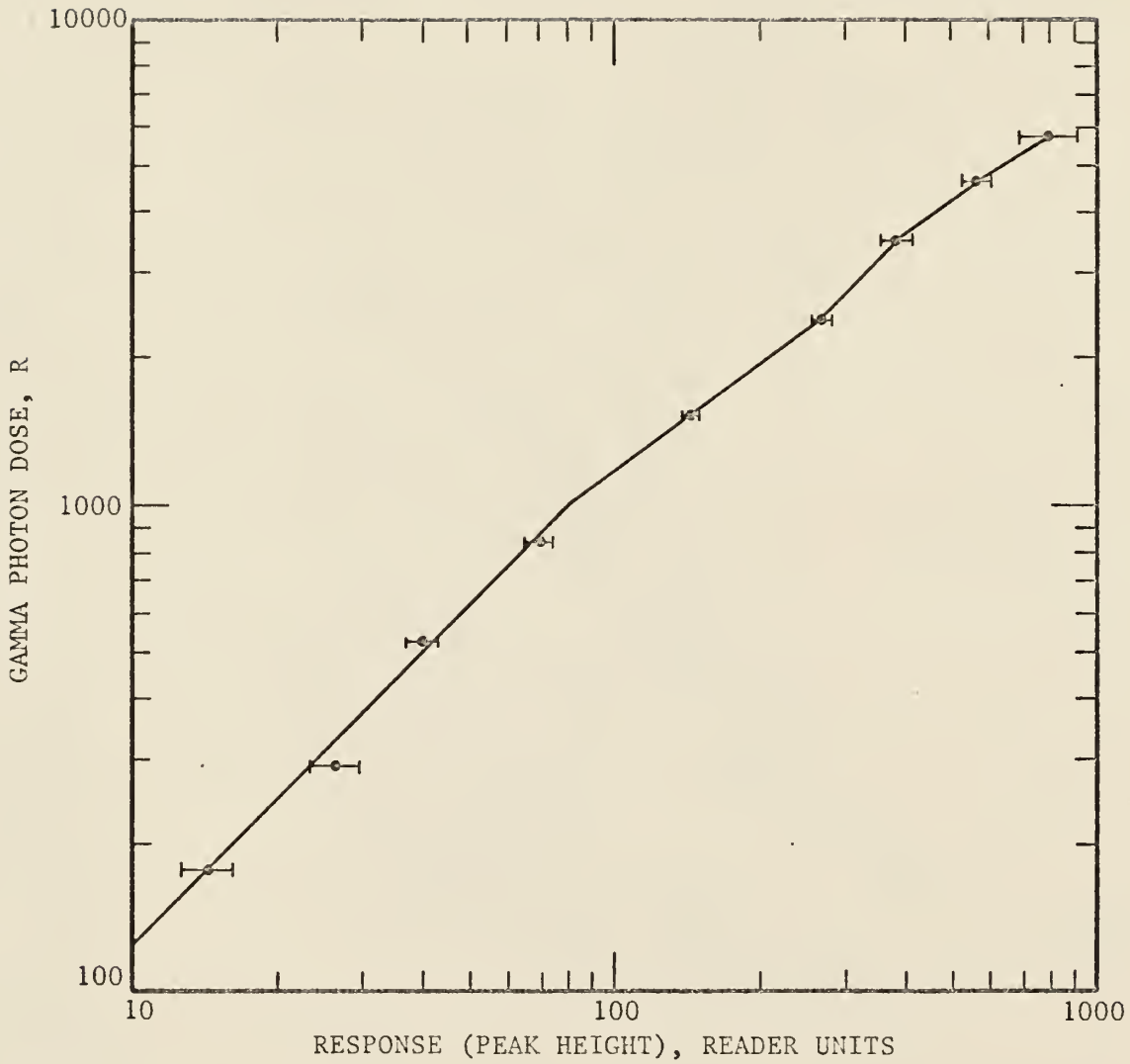

Fig. 21. Gamma calibration curve for EG and G model TL-22 dosimeters in (10^2 to 6 x 10^3) R dose range.(^{6}LiF)

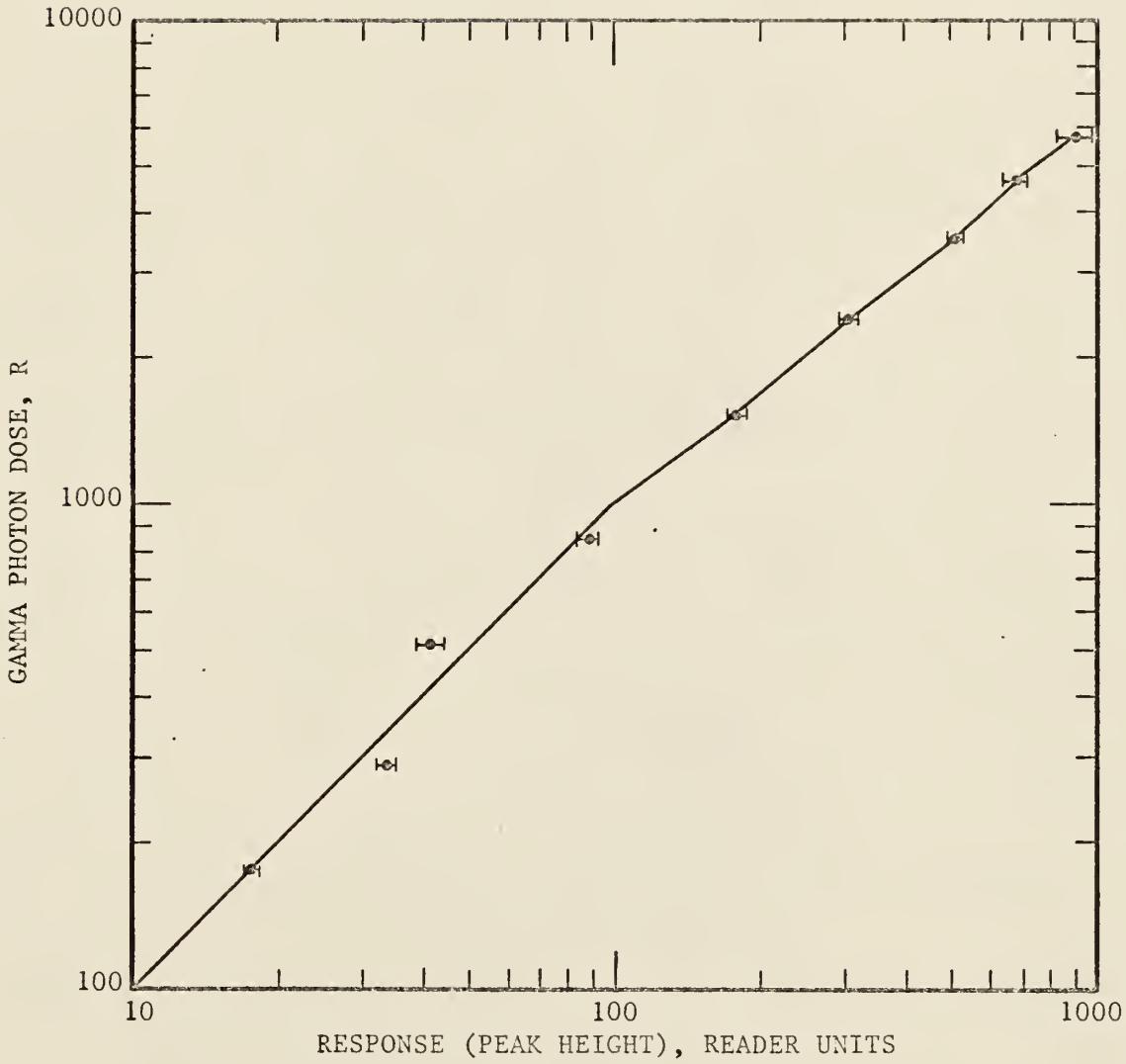

Fig. 22. Gamma calibration curve for EG and G model TL-23 dosimeters in (10^2 to 6 x 10^3) R dose range.(^{7}LiF)

rate of the neutron generator depended upon a number of factors including the deuterium pressure, the extraction voltage, the accelerating potential, the depletion condition of the target, and the position of the irradiation package. Therefore, a dose rate was not exactly reproducible from one irradiation to the next. This was the reason that the foil-activation fluence determination was necessary rather than using charge (beam current x irradiation time) as a relative measure of fluence. Operating conditions during a given irradiation period were relatively constant, but it was very difficult to reproduce the very same operating conditions during a succeeding run. The assumption made in using the foil activation technique was that the neutron flux was constant during a single run.

6.3.2. Experimental Procedure:

The neutron calibration was performed by irradiating nine dosimeter packages for nine different periods of time. Preliminary experimentation had shown the order of magnitude of response obtained for a particular irradiation time, so dosimeters were irradiated over such a range of fluence that the neutron response was of the same order of the response range considered in the gamma calibration. As it turned out, the fluences actually used in neutron irradiation had much higher equivalent tissue doses than the gamma-ray doses which resulted in an equivalent dosimeter response.

The first part of the neutron calibration was performed without the presence of a second package of dosimeters behind

the activation foil and primary dosimeter package. Ten dosimeters, five TL-22's and five TL-23's, were annealed at 400°C for 1 hour prior to irradiation and then placed in a polyethylene package, alternating the two types of dosimeters. Different packages were irradiated for 5, 10, 20, 30, and 40 minutes. The activation foils were removed and counted after a period of two hours to allow decay of the unwanted ^{27}Mg and ^{28}Al products. The foils were placed directly on top of the NaI(Tl) scintillation crystal and counted for a period of time long enough to give approximately 90,000 counts in the 1.37 MeV photopeak. The spectrum data was then used to determine the fluence by the sum-peak method.

Following irradiation, the dosimeters were partially annealed at 110°C for 7 minutes and read out 24 hours after the partial annealing. Since only 5 dosimeters of each type were read out for each irradiation period, the standard deviations of the response values were relatively high. As noted earlier in section 4.3, when ten dosimeters were irradiated side by side, one or two dosimeter responses from each package were generally extremely low. These very low dosimeter responses were eliminated from each data set when necessary, and the mean response and the standard deviation of the mean response were calculated on the basis of four dosimeter readouts.

At this point, new, un-depleted tritium targets were installed in the neutron generator in an effort to obtain a higher range of dosimeter response. To improve the standard

deviation of the response values, irradiation of two dosimeter packages was employed. The dosimeter types were alternated in each package. Irradiation of different packages for periods of 15, 35, 60, and 90 minutes was accomplished. Again the activation foils were removed and counted after a decay period of about two hours. Fluence was determined by the sum-peak method. The dosimeter were partially annealed at 110°C for 7 minutes and read out 24 hours after the partial annealing.

For each irradiation period of 15, 35, 60, and 90 minutes, eight dosimeters of each type were read out. Consistent with the procedure employed in the gamma calibration, the high and low extreme responses were discarded, and the remaining six response values were used to calculate the mean response and the standard deviation of the mean response.

6.3.3. Analysis of Data and Results:

The results of the neutron calibration are presented in Table 9.

Table 9. Data and results for the neutron calibration curves.

Irrad. time, min.	Fluence, 10^9 n/cm^2	TL-22 Response, reader units	TL-23 Response, reader units
5	66.54 ± 7.77	5.01 ± .98	5.56 ± .96
10	176.9 ± 15.7	10.86 ± 2.75	10.13 ± 1.73
20	264.2 ± 8.9	21.77 ± 4.92	21.32 ± 4.70
30	744.9 ± 19.5	61.4 ± 9.1	62.5 ± 7.1

Table 9. Data and results for the neutron calibration curves. (Continued)

Irrad. time, min.	Fluence, 10^9 n/cm^2	TL-22 Response, reader units	TL-23 Response, reader units
40	1177. ± 31.	86.2 ± 24.3	93.8 ± 12.9
15	1919. ± 49.	189.8 ± 23.5	200.3 ± 24.7
35	3279. ± 85.	365.7 ± 74.0	380.7 ± 61.1
60	4599. ± 118.	551.0 ± 58.2	492.5 ± 47.6
90	5450. ± 140.	574.8 ± 79.8	552.2 ± 61.5

For the purpose of this calibration, multiplication of fluence values by a conversion factor for fluence to dose was not performed. Absorbed dose units must be defined for the material in which the absorption occurred, such as tissue dose in rad or rad in LiF. Since the gamma calibration was completed using the exposure dose in R units, fluence rather than absorbed dose was considered a more comparable indication of dose, since neither R nor fluence definitions define the material in which the absorption occurred.

The data of Table 9 were displayed in Figs. 23 and 24. In Fig. 23, the fluence was plotted against the TL-22 response. In Fig. 24, the fluence was plotted against the TL-23 response. A linear least squares analysis was used to fit a straight line through the data points using

$$F = aR + b \qquad (6.3.3\text{-}1)$$

where

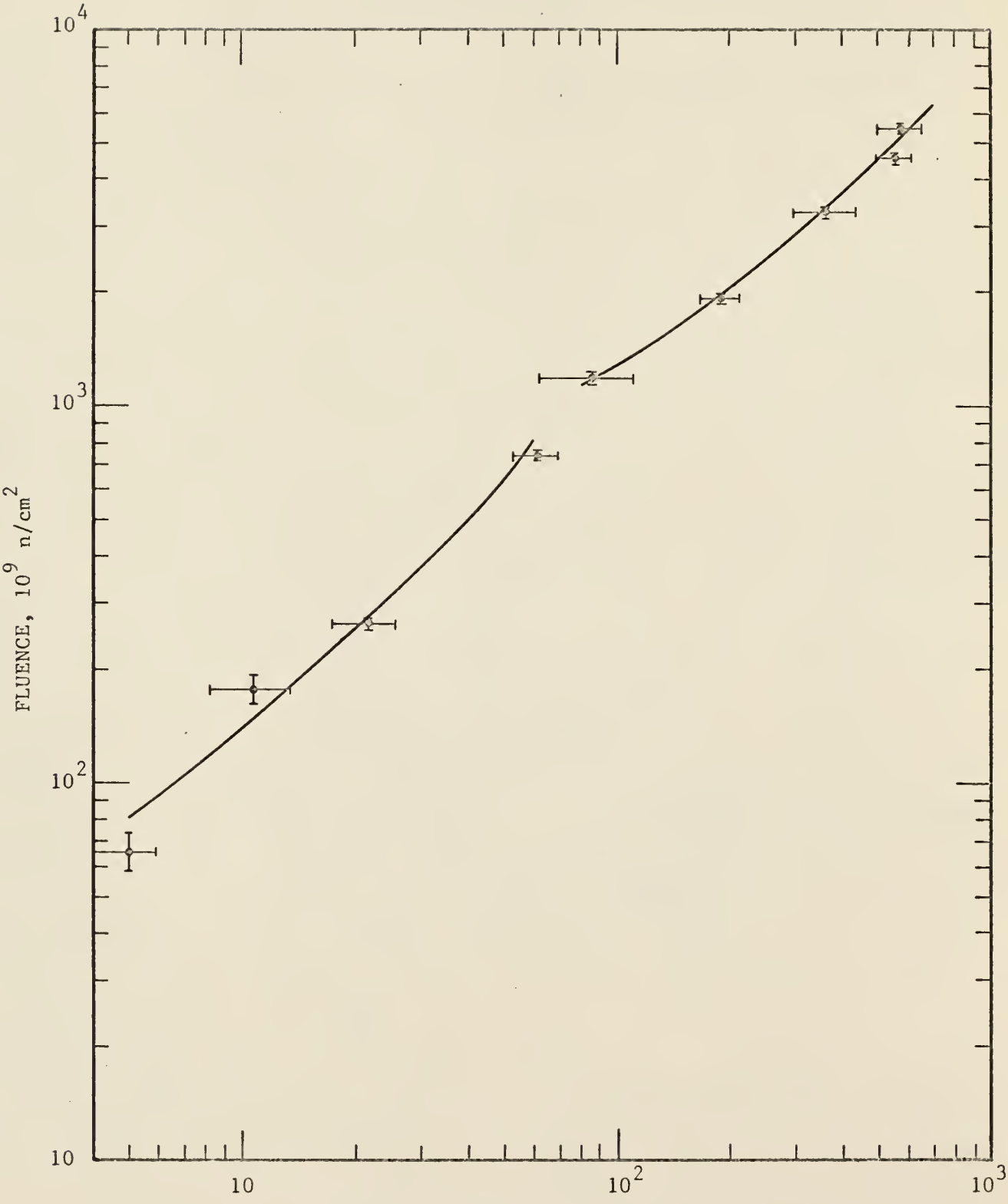

Fig. 23. Neutron calibration curve for EG and G model TL-22 dosimeters in (.6 x 10^{11} to 60 x 10^{11}) n/cm^2 fluence range. (^{6}LiF)

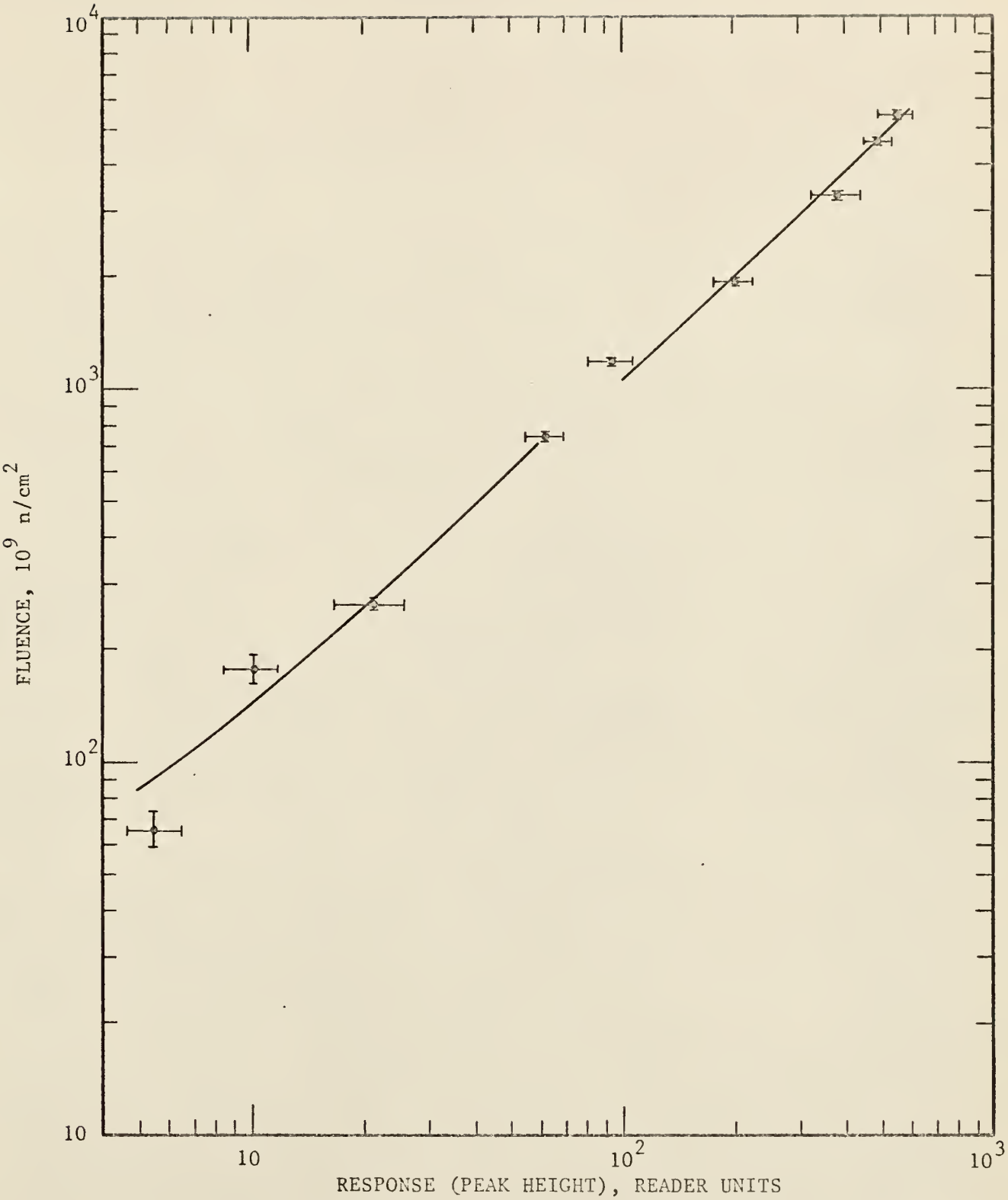

Fig. 24. Neutron calibration curve for EG and G model TL-23 dosimeters in (.6 x 10^{11} to 60 x 10^{11}) n/cm^2 fluence range.(^{7}LiF)

F = fluence, 10^9 n/cm^2,

R = dosimeter response, R.U.,

a = constant, 10^9 n/cm^2, R.U.,

b = constant, 10^9 n/cm^2.

Due to the much greater magnitude of the high response data points, this technique resulted in a poor fit of the lower data points. Therefore, equation (6.3.3-1) was used to fit the data over a lower range and an upper range. The first four data points were used for the lower range, and the last five data points were used for the upper range. For the TL-22 calibration data, the lower range fit resulted in values of a = 11.75 $\pm$ .54 10^9 n/cm^2, R.U. and b = 22.23 10^9 n/cm^2. The upper range fit resulted in values of a = 8.19 $\pm$ .65 10^9 n/cm^2, R.U. and b = 391.37 10^9 n/cm^2. For the TL-23 calibration data, the lower range fit resulted in values of a = 11.49 $\pm$ .66 10^9 n/cm^2, R.U. and b = 27.35 10^9 n/cm^2. The upper range fit resulted in values of a = 9.13 $\pm$ .70 10^9 n/cm^2, R.U. and b = 145.29 10^9 n/cm^2. These least squares lines are also shown in Figs. 23 and 24.

6.4. CORRELATION OF GAMMA AND NEUTRON CALIBRATIONS:

By correlating the gamma calibration and neutron calibration, it was possible to find a neutron fluence and a gamma dose in R that induced equivalent thermoluminescent peak heights. This was possible over the whole range of response values calibrated so that a curve plotting gamma dose in R vs. neutron fluence could be obtained. The results of this correlation are

presented in Figs. 25 and 26 for TL-22 and TL-23, respectively. Fluence values were obtained from the least-squares fits of Figs. 23 and 24. Gamma dose values were obtained using the calibration factor in the range (0 - 10^3R) and graphically above 10^3R.

6.5. DIFFERENCES IN GAMMA AND NEUTRON CALIBRATIONS:

The gamma fading study described in section 5.1 was successful in determining a method which lead to more stable results in readout. However, the partial annealing process adopted was not completely successful in removing the low temperature peaks in the glow curve. Figure 5 showed a typical glow curve for a gamma irradiated dosimeter which had been partially annealed. It was noted during the gamma calibration that there was a good deal of correlation between the height of the main peak and the height of the low temperature peak. This was true for both the TL-22 and TL-23 dosimeters as shown in Table 10.

Table 10. Correlation of main peak and secondary peak heights.

Irrad. Time, sec.	TL-22 Response, R.U.	TL-22 Secondary Peak, R.U.	TL-23 Response, R.U.	TL-23 Secondary Peak, R.U.
0	14.50 ± 1.89	1.30 ± .15	17.57 ± .45	1.22 ± .07
2	26.54 ± 3.27	2.37 ± .21	33.63 ± 1.37	2.34 ± .08
6	40.03 ± 3.39	3.58 ± .18	41.84 ± 2.27	3.23 ± .15
12	70.25 ± 5.05	6.45 ± .34	88.38 ± 3.72	6.98 ± .24
24	144.63 ± 6.55	15.65 ± .64	177.13 ± 8.06	17.44 ± .55
40	269.13 ± 12.05	28.08 ± 2.47	306.63 ± 14.63	30.58 ± 1.54
60	384.38 ± 31.44	20.86 ± 1.41	512.13 ± 14.11	24.21 ± 1.19
80	561.25 ± 38.98	36.5 ± 2.46	683.75 ± 40.33	38.94 ± 1.19
100	798.75 ± 117.65	49.54 ± 4.37	906.11 ± 82.91	48.43 ± 2.65

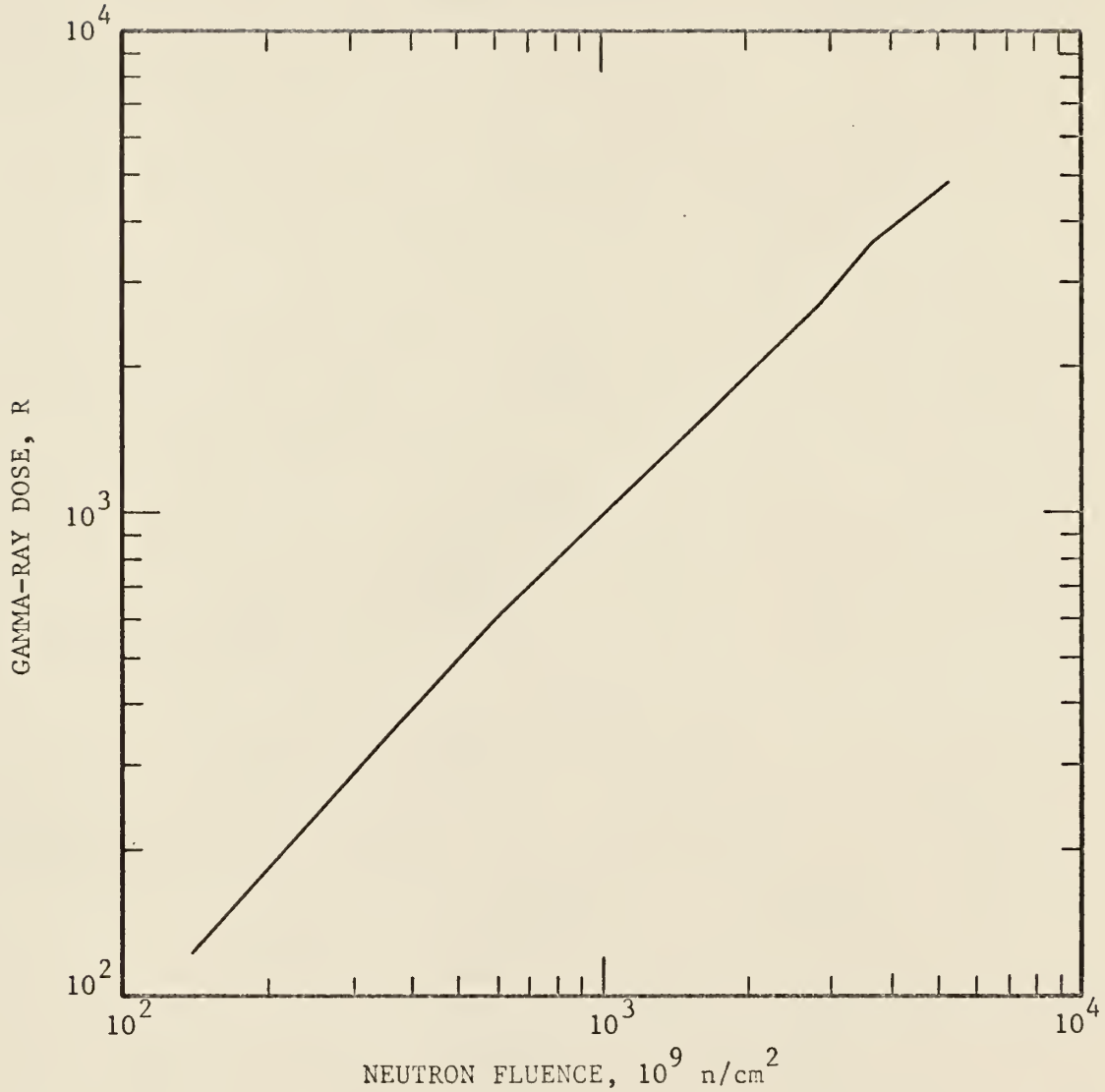

Fig. 25. Gamma dose giving equivalent response to neutron fluence in EG and G model TL-22 dosimeters.(^{6}LiF)

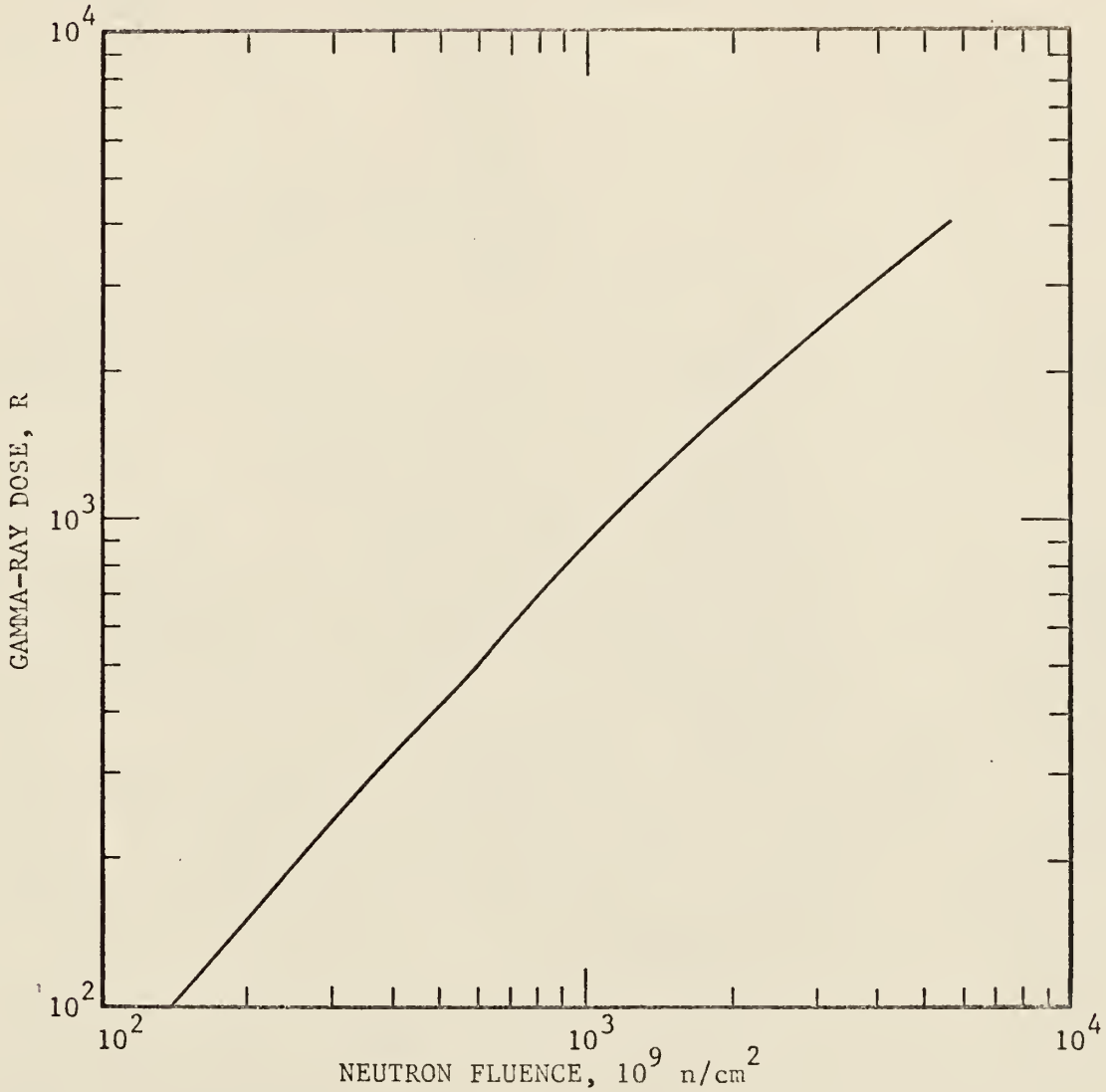

Fig. 26. Gamma dose giving equivalent response to neutron fluence in EG and G model TL-23 dosimeters. (^{7}LiF)

For both the TL-22 and TL-23 dosimeters, the secondary peak height was an increasing function of the dose, up to the dose corresponding to 40 second irradiation time in the Gamma-cell. Above this dose, a depression in the secondary peak height occurred, followed by further increase in the secondary peak height. These data were for a readout performed 24 hours after the partial annealing, and were quite different than that for readout at a different time following the partial annealing.

A typical chart record obtained from a neutron irradiated dosimeter which was partially annealed 24 hours prior to read-out is shown in Fig. 27. It was noted that no secondary peak occurred in the glow curve of a neutron irradiated dosimeter. This was true for both types of dosimeters over the entire response range considered in the neutron calibration.

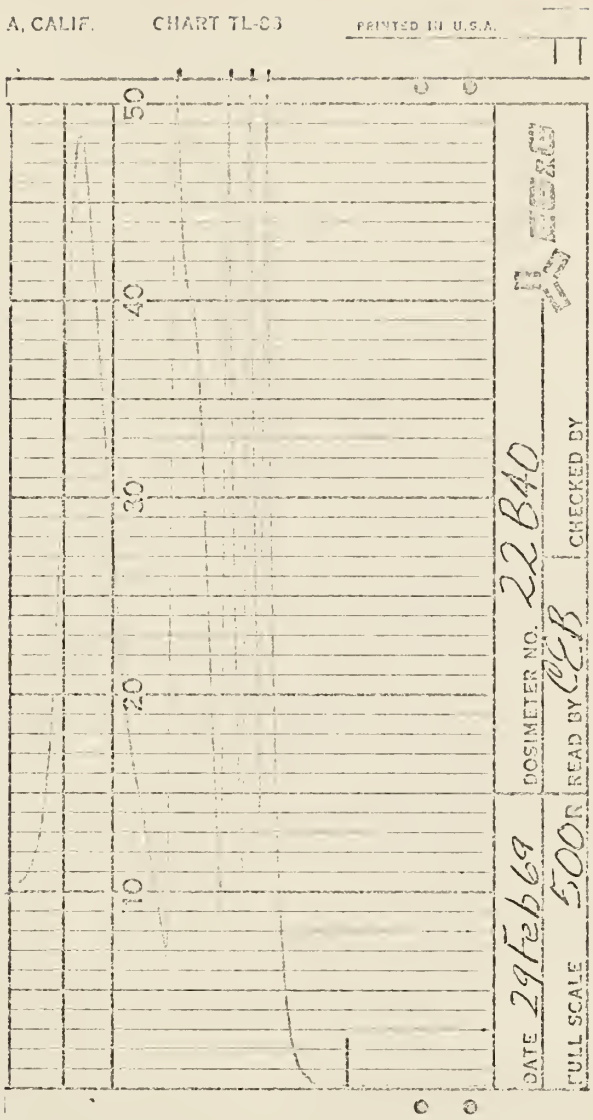

Fig. 27. Typical glow curve for neutron-irradiated dosimeter.

7. DETERMINATION OF COMBINED DOSE EFFECTS

7.1. DETERMINATION OF GENERAL COMBINED RESPONSE CHARACTERISTICS

7.1.1. Basis:

Since both ^{6}LiF and ^{7}LiF thermoluminescent dosimeters are sensitive to both gamma rays and 14.7 MeV neutrons in such a way that the response is an increasing continuous function of the dose, the effect of combined neutron and gamma dose on the response was investigated to determine if the presence of populated traps created by one type of radiation would affect the creation of populated traps by the other type of radiation.

7.1.2. Experimental Procedure:

Twenty-four TL-22 dosimeters were annealed at 400°C for 1 hour. Sixteen of the dosimeters (group A and group B) were irradiated for 50 seconds in the Gammacell. Eight of these dosimeters (group A) were used to monitor the response due to gamma rays alone. The other eight dosimeters (group B) were then packaged in two small polyethylene covers, placed alternately in the packages with eight more dosimeters (group C). Each package contained eight dosimeters, four from group B and four from group C. The packaged dosimeters were then positioned as usual near the neutron generator target behind an activation foil (see section 4.5.2) and neutron irradiated for 65 minutes. All dosimeters were then partially annealed for 7 minutes at 110°C and read out after 24 hours. The same irradiation procedure was repeated using twenty-four TL-23 dosimeters, except

a different tritium target was used, and neutron-irradiation time was 50 minutes instead of 65 minutes.

7.1.3. Results and Conclusions:

Eight dosimeter responses were used to calculate the mean response and standard deviation of the mean response for each group. Group A represented the gamma response, group C represented the neutron response, and group B represented the combined response. The results obtained are presented in Table 11.

Table 11. Response of dosimeters to combined dose.

Dosimeter Type	Neutron Response, R.U.	Gamma Response, R.U.	Combined Response, R.U.
TL-22	319.1 ± 48.6	298.8 ± 38.6	669.4 ± 67.6
TL-23	346.1 ± 54.9	348.1 ± 31.1	805.9 ± 74.7

From the calibration curves (Figs. 21-24), the gamma-ray dose and neutron fluence corresponding to each response value in Table 11 was determined. For TL-22, the neutron response corresponded to a fluence of 3.01×10^{12} n/cm^2, and the gamma response corresponded to a dose of 2.59×10^3 R. For TL-23, the neutron response corresponded to a fluence of 3.31×10^{12} n/cm^2, and the gamma response corresponded to a dose of 2.62×10^3 R.

For TL-22, the experimentally determined combined response mean value of 669.1 ± 67.6 was compared to the calculated combined response value of 617.9 ± 62.1, determined by addition of

the gamma response and the neutron response. For TL-23, the experimentally determined combined response mean value of 805.9 ± 74.7 was compared to the calculated combined response value of 694.2 ± 63.1. For both dosimeter types, the experimental mean response value was slightly larger than the calculated value, but the experimental and calculated values overlapped within the standard deviation.

7.2. DETERMINATION OF EFFECT OF NON-SIMULTANEOUS IRRADIATION

7.2.1. Basis:

Use of dosimeters in combined dose fields would generally take place with simultaneous absorption of the different radiation components. Since separate equipment was used to provide neutron and gamma radiation, it was impossible to determine combined dose effects using simultaneous irradiations. Therefore, experiments were performed to determine the combined dose effects with neutron exposure followed by gamma exposure and with gamma exposure followed by neutron exposure. Section 7.1 showed that the presence of populated traps created by gamma radiation did not affect the creation of populated traps by neutron radiation. Therefore, if the combined response was shown to be the same for neutron dose followed by gamma dose and for gamma dose followed by neutron dose, it could also be concluded that the presence of populated traps created by neutron radiation did not affect the creation of populated traps by gamma radiation. Therefore, the dosimeters could be used in

simultaneous combined radiation fields, knowing the presence of populated traps created by one type of radiation did not affect the creation of populated traps by the other type of radiation.

7.2.2. Experimental Procedure:

Two series of irradiations were performed with both dosimeter types. Sixteen TL-22 dosimeters were irradiated in the Gammacell for 6 seconds. Eight of these dosimeters (group A) were used as a monitor of the response due to the gamma radiation. The other eight dosimeters (group B) were packaged with eight un-irradiated dosimeters (group C) and then neutron irradiated for about 5 minutes (which was calculated to give about the same response due to neutron irradiation). The eight group C dosimeters were then irradiated in the Gammacell for 6 seconds with eight more dosimeters (group D) which served as a monitor of this second gamma irradiation. All twenty-four dosimeters were then partially annealed at 110°C for 7 minutes and read out 24 hours later. This procedure was repeated using TL-23 dosimeters. Then the entire procedure was repeated for both dosimeter types using a Gammacell irradiation time of 50 seconds and a neutron generator irradiation time of approximately 55 minutes.

All dosimeters had been annealed for 1 hour at 400°C prior to irradiation.

7.2.3. Results and Conclusions:

For each dosimeter type, the two series of irradiations covered a relatively low response range and a response range of approximately an order of magnitude higher. Eight response values were used to calculate a mean response and the standard deviation of the mean response. The results obtained are presented in Table 12, along with equivalent gamma dose and neutron fluence for each mean response.

In table 12, the column labeled "B - A Response" represented the response due to neutron irradiation for dosimeters with a prior gamma exposure; the column labeled "C - D Response" represented the response due to neutron irradiation for dosimeters receiving a gamma exposure after neutron irradiation. In each case, the (B - A) mean values were within the standard deviation of the corresponding (C - D) values, and the (C - D) mean values were within the standard deviation of the corresponding (B - A) values. This demonstrated that the response due to neutron radiation was not dependent on whether or not populated traps created by gamma radiation were present, and the response due to the gamma radiation was not dependent on whether or not populated traps created by neutron radiation were present. Thus, the dosimeters could be used in simultaneous combined radiation fields, and the presence of one type of radiation would not affect the response due to the other type of radiation.

Table 12. Response of dosimeters to non-simultaneous combined dose.

a. Pre-neutron gamma irradiation.*

Dosimeter Type	Group A Response, R.U.	Group A Equivalent Dose, R	Group B Response, R.U.	B - A Response, R.U.	B - A Equivalent Fluence, 10^9 n/cm^2
TL-22	50.73 ± 6.48	623.4	91.38 ± 10.03	40.65 ± 11.94	499.9
TL-22	401.8 ± 36.6	3610.	1056.3 ± 142.6	646.5 ± 147.2	5686.
TL-23	52.81 ± 3.63	529.5	91.63 ± 8.45	38.82 ± 9.20	473.4
TL-23	468.5 ± 28.0	3350.	818.1 ± 81.9	349.6 ± 86.6	3337.

b. Post-neutron gamma irradiation.*

Dosimeter Type	Group C Response, R.U.	Group D Response, R.U.	Group D Equivalent Dose, R	C - D Response, R.U.	C - D Equivalent Fluence, 10^9 n/cm^2
TL-22	87.13 ± 9.40	42.50 ± 2.74	522.2	44.63 ± 9.79	547.6
TL-22	946.9 ± 162.2	367.0 ± 30.2	3320.	579.9 ± 165.0	5141.
TL-23	96.50 ± 6.41	51.61 ± 1.69	517.5	44.89 ± 6.63	543.1
TL-23	822.5 ± 55.7	463.8 ± 23.4	3300.	358.7 ± 60.4	3420.

*Group A = pre-neutron gamma irradiation
Group B = pre-neutron gamma irradiation and neutron irradiation
Group C = neutron irradiation and post-neutron gamma irradiation
Group D = post-neutron gamma irradiation
B - A = response due to neutron irradiation for group B dosimeters
C - D = response due to neutron irradiation for group C dosimeters

7.3. EFFECT OF COMBINED DOSE ON SECONDARY PEAK:

The correlation between the low temperature peak and the main peak in the glow curve, which was described in section 6.5, did not appear for combined dose radiations. The secondary peak did appear in combined dose glow curves, but it was not in the same proportion to the main peak as it was for gamma radiation alone, nor was it the same magnitude as it was for a gamma radiation of the same dose used in the combined radiation.

8. DISCUSSION AND CONCLUSIONS

8.1. DISCUSSION OF PRELIMINARY EXPERIMENTS:

The gamma-ray background on the neutron generator was determined to be slightly larger in terms of percentage for TL-23 dosimeters, since the neutron response of TL-23 dosimeters was lower, and the gamma response was higher than the corresponding responses of the TL-22 dosimeters. In either case, the response due to gamma rays did not exceed 2% of the response due to neutrons. The primary gamma-ray dose received during irradiation was due to the $^{27}Al(n,\gamma)^{28}Al$ reaction in the activation foil and the accelerator cap. The short half life of this product resulted in attainment of saturation activity in a relatively short time, so that for irradiation periods of greater than about 15 minutes, the slight increase in the gamma response as a percentage of the neutron response was due to the buildup of the two other products, ^{24}Na and ^{27}Mg. By keeping a detailed record of irradiations performed, it would have been possible to estimate the gamma-ray contamination received by each set of neutron-irradiated dosimeters. This was not done, due to the limited number of dosimeters available and the additional computer time which would have been necessary to perform trapezoidal integrations to relate post-neutron irradiation response to response during irradiation (procedure as described in section 5.2). For most irradiations, the gamma response was between 1% and 2% of the neutron response.

The results of the fading study lead to the adoption of the post-irradiation procedure described in section 5.1.3. When gamma-irradiated dosimeters were read out 24 hours after post-irradiation annealing, there was a good deal of correlation between secondary peak height and main peak height. The fading study glow curves showed, however, that the secondary peak decayed considerably over the 72 hour fading study period, and the correlation between the secondary peak and the main peak was greatest at the 24 hour readout time.

The partial annealing procedure produced low main peak response for TL-22 dosimeters read out 1.5 hours after partial annealing. This suggested that an equilibrium process was involved between low temperature and high temperature traps in ^{6}LiF. The process evidently either did not occur in ^{7}LiF, or equilibrium was attained sooner than 1.5 hours after the partial annealing.

8.2. DISCUSSION OF CALIBRATION EXPERIMENTS:

Over the range 0 to 10^{3} R, the calibration factors obtained for conversion of response (reader units) to gamma-ray dose (R) were 12.288 R/R.U. and 10.027 R/R.U. for TL-22 and TL-23 dosimeters, respectively. Thus for a dose in this range, the TL-23 response would be about 23% higher than the TL-22 response. In the range above 10^{3} R, the TL-23 response was higher at each calibration dose by a factor of from 14% to 33%, averaging 20% higher. It has been reported that the responses of ^{6}LiF and ^{7}LiF to gamma-ray dose are essentially

identical[3]. Evidently the higher gamma-ray response obtained for the TL-23 dosimeters used in these experiments was due to grouping by the manufacturer. After a standardized irradiation, dosimeters were grouped by the manufacturer to be within ±10% of the mean response. The group of TL-23 dosimeters evidently had a mean response of about 20% higher than the mean response of the TL-22 dosimeters. This was probably due to slight differences in the amount of phosphor in the ampule.

The least squares fit in the low response range of the neutron calibration using equation (6.3.3-1), $F = aR + b$, resulted in values of $a = (11.75 \pm .54) \times 10^9$ n/cm^2, R.U. and $b = 22.23 \times 10^9$ n/cm^2 for TL-22, and $a = (11.49 \pm .66) \times 10^9$ n/cm^2, R.U. and $b = 27.35 \times 10^9$ n/cm^2 for the TL-23 dosimeters. It thus appeared that the neutron responses of the TL-22 and TL-23 dosimeters were very nearly identical in the low response range. However, to adjust for the greater amount of phosphor contained in each TL-23 dosimeter, the neutron response of TL-23 dosimeters should be reduced by about 20% to obtain TL-23 response due to a quantity of phosphor equivalent to the quantity of phosphor in the TL-22 dosimeters.

As described in section 6.3.2, the neutron calibration was performed over the same response range as the gamma calibration, without regard to the actual tissue dose received in the neutron irradiation. For gamma-ray radiation, LiF is nearly tissue equivalent, but for neutron radiation, it is not. A response of 50 reader units, for instance, corresponded to a

gamma-ray dose of 614.4 R or 609.7 x 10^9 n/cm^2 for the TL-22 dosimeters and corresponded to a gamma-ray dose of 501.4 R or 601.5 x 10^9 n/cm^2 for the TL-23 dosimeters. From ref. (27), the conversion factor for R to tissue rad is .965 tissue rad/R. From ref. (28), the conversion factor for 14.7 MeV fluence to first collision dose in tissue rad is 6.06 x 10^{-9} rad/(n/cm^2). Therefore, the dose in tissue which gave a TL-22 response of 50 reader units was 592.9 rad ^{60}Co gamma dose or 3695 rad 14.7 MeV neutron dose. The dose in tissue which gave a TL-23 dosimeter response of 50 reader units was 483.9 rad gamma dose or 3647 rad 14.7 MeV neutron dose. (A set of dose values inducing equivalent responses could be obtained from Figs. 25 and 26 by considering responses other than 50 reader units.) Based on the response of 50 reader units, the TL-22 dosimeters were more sensitive to ^{60}Co gamma rays than to 14.7 MeV neutrons by a factor of approximately 6.23, based on equivalent tissue dose. The TL-23 dosimeters were more sensitive to ^{60}Co gamma rays than to 14.7 MeV neutrons by a factor of approximately 7.70.

8.3. CONCLUSIONS:

Several conclusions can be drawn based upon the results of these studies.

(1) The postirradiation annealing process (7 minutes at 110°C) has a different effect on ^{6}LiF thermoluminescent dosimeters and on ^{7}LiF thermoluminescent dosimeters.

(2) Gamma-ray irradiation of both ^{6}LiF and ^{7}LiF dosimeters followed by postirradiation annealing results in lower-temperature traps. For neutron irradiation, no such traps appear.

(3) The response of ^{7}LiF thermoluminescent dosimeters to 14.7 MeV neutrons is lower by about 20% than the response of ^{6}LiF thermoluminescent dosimeters to an equivalent neutron dose.

(4) On a tissue dose basis, TL-22 dosimeters are approximately 6.2 times as sensitive to ^{60}Co gamma rays as to 14.7 MeV neutrons. TL-23 dosimeters are about 7.7 times as sensitive to ^{60}Co gamma rays as to 14.7 MeV neutrons.

(5) In a mixed radiation field of 14.7 MeV neutrons and ^{60}Co gamma rays, the presence of populated traps created by one type of radiation does not inhibit the creation of populated traps by the other type of radiation in either ^{6}LiF or ^{7}LiF.

9. SUGGESTIONS FOR FURTHER STUDY

In the field of thermoluminescent dosimetry, many areas still need investigating.

The neutron energy dependence of the response of ^{6}LiF and ^{7}LiF dosimeters needs further investigation over a wide range of neutron energies.

Since the lower-temperature peak did not appear in the glow curve of neutron-irradiated dosimeters, a fading study of neutron-irradiated dosimeters would be quite interesting, as a key to the actual cause of fading in gamma-irradiated dosimeters. This would require a source of neutrons capable of accurate reproduction of the dose received by the many dosimeters required for a fading study.

The availability of a neutron source to accurately reproduce the dose received by many dosimeters would also enable study of different gamma-ray doses applied over a given level of neutron dose. From this study, perhaps some correlation could be found between the gamma dose and the secondary peak height for a dosimeter which received a combined dose.

Determination of the differences in the thermoluminescent emmission spectra of ^{6}LiF and ^{7}LiF for gamma radiation and neutron radiation might indicate the mechanisms responsible for the differences in the glow curves of neutron and gamma-irradiated dosimeters.

10. ACKNOWLEDGEMENT

The author is indebted to many people who aided in the completion of this work: to Dr. Hermann J. Donnert for his continuous guidance and encouragement; to Dr. N. D. Eckhoff for his instruction and suggestions with the experimental work; to Pat Ervin and Joe McCleskey for their cooperation; and to Ray Hightower for his help with the experimental equipment. The author is grateful to them all.

Financial support from the National Aeronautics and Space Administration and the Department of Defense Themis Project, administered through the Office of Naval Research, is gratefully acknowledged.

11. LITERATURE CITED

1. Z. Spurny, "Thermoluminescent dosimetry," At. En. Rev. 3, 61 (1965).

2. F. Daniels, C. A. Boyd and D. F. Saunders, "Thermoluminescence as a research tool," Science 117, 343 (1953).

3. C. Distenfeld, W. Bishop and D. Colvett, "Thermoluminescent neutron-dosimetry system," CONF-650637, AEC symposium series 8, 457 (1967).

4. G. W. R. Endres, "Thermoluminescent dosimetry studies at Hanford," CONF-650637, AEC symposium series 8, 435 (1967).

5. C. L. Wingate, E. Tochilin and N. Goldstein, "Response of LiF to neutrons and charged particles," CONF-650637, AEC symposium series 8, 421 (1967).

6. P. S. Weng, "Lithium fluoride thermoluminescent response to neutrons," IEEE Transactions Nucl. Sci. NS-13, 222 (1966).

7. J. J. Brophy, Basic Electronics for Scientists, (McGraw-Hill Book Company, Inc., New York, 1966).

8. "TL dosimetry system, Models TL-38 and TL-3C," Operation Manual, #S-316-MN, EG and G Santa Barbara Division (1966).

9. J. H. Schulman, "Survey of luminescence dosimetry," CONF-650637, AEC symposium series 8, 3 (1967).

10. S. G. Gorbics, "Emission spectra of various thermoluminescent materials," CONF-650637, AEC symposium series 8, 167 (1967).

11. E. W. Claffy, "Thermoluminescence and color centers in LiF," CONF-650637, AEC symposium series 8, 74 (1967).

12. C. C. Klick, E. W. Claffy, S. G. Gorbics, F. H. Attix, J. H. Schulman and J. G. Allard, "Thermoluminescence and color centers in LiF:Mg," J. Appl. Phys. 38, 3867 (1967).

13. C. A. Boyd, "Kinetic study of thermoluminescence of LiF," J. Chem. Phys. 17, 1221 (1949).

14. J. R. Cameron, F. Daniels, N. M. Johnson and G. Kenney, "Radiation dosimeter utilizing the thermoluminescence of LiF," Science 134, 333 (1961).

15. G. A. Brinkman, A. H. W. Aten and J. T. Veenhoer, "Absolute standardization with a NaI(Tl) crystal - I," Int. J. App. Rad. and Isotop. 14, 153 (1963).

16. D. W. Zimmerman, C. R. Rhyner and J. R. Cameron, "Thermal annealing effects on the thermoluminescence of LiF," CONF-650637, AEC sumposium series 8, 86 (1967).

17. M. Kaiseruddin, "Effects of very high dose rates of the response of LiF thermoluminescent dosimeters," M. S. Thesis, Kansas State University, Department of Nuclear Engineering, 1968.

18. C. J. Karzmark, J. F. Fowler and J. T. White, "Problems of reader design and measurement error in LiF thermoluminescent dosimetry," Int. J. App. Rad. Isotop. 17, 161 (1966).

19. J. R. Cameron, D. W. Zimmerman and R. W. Bland, "Thermoluminescence vs. roentgens in LiF: a proposed mathematical model," CONF-650637, AEC symposium series 8, 47 (1967).

20. N. P. Dean and J. H. Larkins, "Thermoluminescent dosimetry with activated LiF," AEC report LAMS-3034, 205 (1963).

21. F. F. Morehead and F. Daniels, "Thermoluminescence and coloration of LiF produced by alpha particles, electrons, gamma rays and neutrons," J. Chem. Phys. 27, 1318 (1957).

22. J. Kastner, B. G. Oltman and P. Tedeschi, "LiF thermoluminescent response to fast neutrons," Health Phys. 12, 1125 (1966).

23. D. J. Hughes and R. B. Schwartz, "Neutron Cross Sections," BNL-325, 2nd ed., Brookhaven National Laboratory, (1958).

24. B. G. Oltman, J. Kastner, P. Tedeschi and J. N. Beggs, "The effects of fast neutron exposure on the LiF thermoluminescent response to gamma rays," Health Phys. 13, 918 (1967).

25. J. T. Prud'homme, "Texas Nuclear Corporation Neutron Generators," Texas Nuclear Corp., Subsidiary of Nuclear-Chicago Corp., Austin, Texas (1962).

26. J. R. Stehn, M. D. Goldberg, B. A. Magurno and R. Wiener-Chasman, "Neutron Cross Sections," BNL-325, 2nd ed., supp. #2, Brookhaven National Laboratory, (1964).

27. H. Goldstein, Fundamental Aspects of Reactor Shielding, (Addison-Wesley Publishing Company, Inc., Reading, Mass., 1959).

28. "Measurement of absorbed dose of neutrons and of mixtures of neutrons and gamma rays," NBS Handbook 75, (1961).

29. N. D. Eckhoff, "Optimal Neutron Activation Analysis," Ph.D. Thesis, Kansas State University, Department of Nuclear Engineering, 1968.

30. P. C. Stevenson, "Processing of Counting Data," NAS-NS-3109, (1965).

31. C. R. Wiley, Advanced Engineering Mathematics, (McGraw-Hill Book Company, Inc., New York, 1966).

12. APPENDIX A

CURVE FITTING METHOD

The following method was used in this work to fit the two photo-peaks and the sum peak of the ^{24}Na-decay spectra to a Gaussion function.

The peaks were assumed to be pure Gaussian, i.e.,

$$Y_i = Y_o \, e^{\frac{-(x_i - x_o)^2}{b_o}} \qquad \text{(A-1)}$$

where

Y_i = counts in channel i of photopeak,

Y_o = count corresponding to channel x_o,

x_o = mean channel of the Gaussian function,

x_i = channel number,

$b_o = 2\sigma^2$

σ^2 = variance of the Gaussian function.

Equation (A-1) is nonlinear and must be linearized to apply the principle of least squares. The logarithm of equation (A-1) yields a linear form:

$$\ln Y_i = \ln Y_o - \frac{x_o^2}{b_o} + \frac{2x_o}{b_o} x_i - \frac{1}{b_o} x_i^2 \qquad \text{(A-2)}$$

Equation (A-2) can be written in terms of new variables:

$$z_i = a_1 + a_2 x_i + a_3 x_i^2, \qquad \text{(A-3)}$$

where

$$z_i = \ln Y_i$$

$$a_1 = \ln Y_o - \frac{x_o^2}{b_o}$$

$$a_2 = \frac{2x_o}{b_o}$$

$$a_3 = -\frac{1}{b_o}$$

The principle of least squares applied to equation (A-3) yields the following matrix equation [29]:

$$\underline{a} = (\underline{X}'\underline{W}\,\underline{X})^{-1}\,(\underline{X}'\underline{W}\,\underline{Z}), \qquad \text{(A-4)}$$

where

$\underline{a}$ is a (3 x 1) vector of the coefficients a_1, a_2, and a_3,

$\underline{X}$ is a (n x 3) matrix whose first column is composed of all unity values, the second column is composed of the x_i values, and the third column is composed of the x_i^2 values,

$\underline{X}'$ is the traspose of $\underline{X}$,

$\underline{Z}$ is a (n x 1) vector of the z_i values,

$\underline{W}$ is a (n x n) diagonal weighting matrix whose elements are the inverse of the variances of the Z_i values,

n is the number of data points.

The variance of Z_i can be obtained by [30]:

$$\sigma^2(Z_i) = \frac{1}{Y_i^2}\,\sigma^2(Y_i) \doteq \frac{1}{Y_i}. \qquad \text{(A-5)}$$

It should be noted that by applying the principle of least squares to equation (A-3) instead of to equation (A-1), the minimum total squared deviation is

$$S_L = \sum_{i=1}^{n} \{\ln Y_i - (\ln Y_o - \frac{x_o^2}{b_o} + \frac{2x_o}{b_o}x_i - \frac{1}{b_o}x_i^2)\}^2. \qquad \text{(A-6)}$$

The desired minimum total squared deviation is

$$S_D = \sum_{i=1}^{n} \{Y_i - Y_o\, e^{\frac{-(x_i - x_o)^2}{b_o}}\}^2 \qquad \text{(A-7)}$$

Minimumizing S_L does not guarantee a minimum for S_D[31]. To minimize S_D requires an iterative technique which employs a Taylor's series expansion and can result in unstable solutions for cases with variations in the data. In addition, this method requires a significantly longer amount of computation time.

Variance values for Y_o, x_o, and b_o were obtained by:

$$\sigma^2(Y_o) = \{C_{1,1} + \frac{a_2^2}{4a_3^2}(C_{2,2} + \frac{a_2^2}{4a_3^2}C_{3,3})\}\exp\{2(a_1 - \frac{a_2^2}{4a_3})\} \qquad \text{(A-8)}$$

$$\sigma^2(x_o) = \frac{1}{4a_3^2}\{C_{2,2} + (a_2/a_3)^2 C_{3,3}\} \qquad \text{(A-9)}$$

$$^2(b_o) = C_{3,3}/a_3^4 \qquad \text{(A-10)}$$

where

a_1, a_2, and a_3 are the elements of the vector $\underline{a}$,

and

$C_{1,1}$, $C_{2,2}$, and $C_{3,3}$ are the diagonal elements of the $(\underline{X}'\underline{W}\,\underline{X})^{-1}$ matrix.

Since the Y_o value is just a normalization term, it could also be calculated by minimizing S_D after x_o and b_o were obtained by minimizing S_L. This method yielded lower variance values for Y_o. Hence, Y_o and $^2(Y_o)$ were calculated from

$$Y_o = \frac{\sum_{i=1}^{n} W_i Y_i K_i}{\sum_{i=1}^{n} W_i K_i^2} \qquad \text{(A-11)}$$

$$\sigma^2(Y_o) = \frac{1}{\sum_{i=1}^{n} W_i K_i^2} \qquad \text{(A-12)}$$

where

n = the number of data points used in the fit,

$$K_i = \exp\{-(x_i - x_o)^2/b_o\}$$

In deriving equation (A-12), it was assumed that $W_i \doteq 1/Y_i$.

Having determined the parameters of the Gaussian Function, the area of the peak was determined by integration of equation (A-1) from $-\infty$ to $+\infty$. The area was given by

$$A = Y_o(\pi b_o)^{\frac{1}{2}} \qquad \text{(A-13)}$$

Photofit Code -- Programmed By Eckhutt -- Modified By Bliss

```
FORTRAN IV G LEVEL 1, MOD 3            MAIN              DATE = 69080        14/21/40          PAGE 0001

0001            D)MEMS)UNSPECT(256),      BKG(256),VAR(256),A(3,3),B(3),O(20),Z(10
                1),VAR1(256),SPEC1(256),C(256,E)10),CI(256),AREAS(3),CC(3),BKGM(25
                26)
0002             1 FORMA((4)3)
0003             2 FORMAT(6X,I2F6.0,2X)
0004             3 FORMAT(5E14.8)
0005             4 FORMA((/3X,7H ENERGY,13X,3H YO,13X,3H XO,13X,3H BO,12X,5H FWHM,8X
                 [,11H RESOLUT)ON,8X,5H AREA /)
0006             5 FORMAT(20A4)
0007             7 FORMAT( E14.8,4X,E14.8,2X,E14.8,2X,E14.8,2X,E14.8,2X,E14.8,2X,E14
                 (.8)
0008             8  FORMA(( 8X,)3.7X,E(4.8,10X,E14.8 )
0009             9  FORMAT( // 5X,8H CHAMMEL,10X,9H SPECTRUM,10X,16H WTS(LOG OOMAIN)
                 I/)
0010            10 FORMAT(1HI)
0011            11 FORMAT(15X,29H COMPTOM EOGE MINUS GAUSS FIT )
0012            12  FORMAT( // 5X,8H CHANNEL,10X,9H SPECTRUM,10X,16H WTS(LIM OOMAIN)
                 1/)
0013            13 FORMA(//1OH SIAND OEV /)
0014            14 FORMA(( /// 10X,8H SLOPE = ,E14.6,10X,12H INTERCEPT = ,E14.6 /  )
0015            15 FORMA(// 15X,33H PHOTO PEAK MINUS EXPONENTIAL FIT )
0016            17 FORMAT(8F10.6)
0017            18 FO4MA((1H1,7H   AI = ,F12.6,7H   A2 = ,F12.6,8H   AI2 = ,E12.6,10H
                 1   TOTAL = ,F12.6,'   OISINTEGRATIONS =',F(2.6)
0018            19 FORMAT(2F4.0)
0019            20 FORMAT(5A4,4F10.5)
0020            21 FORMA((5A4)
0021            22 FORMAT(1HO,6X,'O)SINTEGRATIONS PER GRAM =',E14.6)
0022            24 FORMA((1HO,6X,'ZERO TIME U)S(MTEGRAIIONS =',E14.6)
0023            25 FORMAT(1HO,6X,'IRRAO TIME =',F8.4,'   COUNT TIME =',F8.4,'   OECAY
                 1 TIME =',F8.4,'   CORR OECAY TIME =',F8.4)
0024            26 FORMAT(1HO,14X,'TOTAL M/SO.CM. =',E16.8,'      STO. DEV. =',E16.8)
0025            27 FORMAT(8F10.5)
0026            28 FORMAT(I4,F4.0)
0027            29 FORMAT(1HO,14X,'VAR1 = ',E16.8,'  VAR2 = ',E16.8,'  VAR3 = ',E16.8
                 I)
0028            30 FORMAT(1HO,14X,'VARF1 = ',E16.8,'  VARF2 = ',E16.8)
                C
                C********* ALL VARIANCES IN THE LOG OOMAIN
                C**********NOSPEC IS THE NUMBER OF SPECTRA USING THE SAME BKG
                C       STIME IS THE COUNTING TIME FOR THE SPECTRUM
                C       BTIME IS THE COUNTING TIME FOR THE BACKGROUNO
                C       HTIME = ZERO IF THERE IS NO BACKGROUNO COUNTING TIME
                C      TR = TIME FROM REMOVAL TO BEGINNING OF COUNT
                C      TIRR = IRRAOIATION TIME
                C      ALL TIMES EXPRESSEO IN MINUTES
                C
                C
                C**********MOOE=1 INPUT BY 6X,12F6.0,2X
                C                2 INPUT BY 8F10.0
                C********** KINO=1 BKG IS NOT SUBTRACTEO
                C                2 BKG IS SUBTRACTED
                C********* MPEAK IS THE NUMBER OF PEAKS TO BE FIT PER SPECTRUM
                C
0029            100 READ(1,28)NOSPEC,BTIME
0030                BTIME=BTIME/60.
0031                IF(NOSPEC.EO.0)CALL EXIT
0032                OO 704 II=1,NOSPEC


FORTRAM IV G LEVEL 1, MOO 3            MAIN              DATE = 69080        14/21/40          PAGE 0002

0033                READ(1,20)IO(I),I=1,5),WEIGHT,STIME,TIRR,(R
0034                STIME=STIME/60.
0035                (IRR=IIRR/60.
0036                IR=TR/60.
0037            110 READ(I,I)NCHM,MOOE,KINO,MPEAK
0038                READ(I,27)(E(I),I=1,NPEAKI
0039            101 IF(I).GT.1)GOTU119
0040                IF(MOOE.EO.2).AND.(KINO.EO.1))GO TO I21
0041                IF(MOOE.EO.2)GO TO 112
0042                )F((MOOE.EQ.1).ANO.(KINO.EO.I))GOIO120
0043            111 READ(1,2)(BKG(J),J=1,MCHN)
0044                GOTO118
0045            112 READ(I,17)(BKG(J),J=1,NCHM)
0046            118 OO 1201J=1,NCHN
0047           1201 BKGM(J)=BKG(J)
0048            119 CONTINUE
0049                IF(MOOE.EO.2)GO TO I21
0050            120 READ(1,2)(SPECT(J),J=I,NCHM)
0051(               IF(KINO.EO.1)GOTOT301
0052                GO TO 130
0053            121 READ(1,17)(SPECT(J),J=I,NCHN)
0054                IF(KIMO.EQ.I)GOTO1301
0055            130 CONTINUE
0056                FACT=STIME/BTIME
0057                OO1300 J=1,NCHM
0058                SPECT(JI=SPECT(JI-BKGM(J)*FACT
0059                IF(SPECT(JI.LT.0.0)GOTOI303
0060                GOTOI300
0061           1303 SPECT(J)=0.0
0062           I300 CONTINUE
0063           I301 (AREA=0.0
0064                OOI33 J=1,NCHN
0065            I33 TAREA=TAREA+SPECT(J)
0066           1302 OO 700 JJ=1,NPEAK
                C
                C********* IPPLL IS (HE LOWER LIMIT OF THE PEAK
                C********* IPPUL IS THE UPPER LIMIT OF THE PEAK
                C*********NCOMP IS THE FIRST OATA POINT OF THE COMPION EOGE
                C**********LINE IS THE LAST OATA POINT USEO IM THE EXPONENTIAL
                C*********LEAST SQUARES FII
                C
0067                READ(I,5)(O(I),I=1,20)
0068                WRITE(3,10)
0069                WRITE(3,5)IO(I),I=1,20I
0070                WR)TE(3,9)
0071            140 READ(I,I)IPPLL,IPPUL,NCOMP,LINE
0072                OO 132 J=MCOMP,IPPUL
0073                IF(KINO.EO.1)GO TO 131
0074                VAR(J)=((SPECT(J)-FAC)*BKGM(JI)**2)/(SPECT(J)+BKGM(J)*FACT**2)
0075                IF(KINO.E0.2)GU TO 132
0076            I31 VAR(J)=SPECT(J)
0077            I32 CONTINUE
0078                WRITE(3,8)(J,SPECT(J),VAR(J),J=MCOMP,IPPUL)
0079                OOIOOO J=NCOMP,IPPUL
0080                VAR1(J)=VAR(J)
0081           1000 SPECI(J)=SPECT(J)
0082            141 AREAO=0.
0083            142 CALL GAUSSI(SPECT,NCHN,)PPLL,)PPUL,BO,YO,XO,AREA,C,VAR,A,B)
```

```
FORTRAN IV G LEVEL 1, MOD 3            MAIN              DATE = 69080        14/21/40            PAGE 0003

0084          145 W=1.644*SQRT(80)
0085              R=W*100./X0
0086              WRITE(3,4)
0087              WRITE(3,7)E(JJ),Y0,X0,B0,W,R,AREA
0088              WRITE(3,13)
0089              WRITE(3,7)E(JJ),C(3),C(1),C(2),C(4),C(5),C(6)
0090              CC(JJ)=C(6)
0091              AREAS(JJ)=AREA
0092              GOTO700
0093               IF(JJ.EQ.3)GOTO700
          $
       01)  (EY002I LABEL
0094              RAT=AREA0/AREA
0095              IF((0.950.LT.RAT).AND.(1.050.GT.RAT))GO TO 700
0096              AREA0=AREA
             C
             C******** SUBTRACT FIT FROM COMPTON EDGE
             C
0097              WRITE(3,10)
0098              WRITE(3,11)
0099              WRITE(3,12)
0100              DO 150 K=NCOMP,LINE
0101              C(K)=Y0*EXP((-(FLOAT(K)-X0)**2)/B0)
0102              BKG(K)=((SPECT(K)-C(K))**2)/SPECT(K)
0103          150 C(K)=ALOG(SPECT(K)-C(K))
0104              WRITE(3,8)IK,C(K),BKG(K),K=NCOMP,LINE)
             C
             C******** FORM SOLUTION MATRIX
             C
0105              XK=0.
0106              DO 200 I=1,2
0107              B(I)=0.
0108              DO 200 J=1,2
0109          200 A(I,J)=0.
0110              DO 210 K=NCOMP,LINE
0111              A(1,1)=A(1,1)+BKG(K)
0112              A(1,2)=A(1,2)+XK*BKG(K)
0113              A(2,2)=A(2,2)+(XK**2)*BKG(K)
0114              B(1)=B(1)+C(K)*BKG(K)
0115              B(2)=B(2)+XK*C(K)*BKG(K)
0116          210 XK=XK+1.
0117              A(2,1)=A(1,2)
0118              SLOPE=(A(1,1)*B(2)-A(2,1)*B(1))/(A(1,1)*A(2,2)-A(2,1)*A(1,2))
0119              CEPT=EXP((B(1)*A(2,2)-B(2)*A(1,2))/(A(1,1)*A(2,2)-A(2,1)*AI1,2)))
0120              CEPT=CEPT*EXP(-SLOPE*FLOAT(NCOMP))
0121              WRITE(3,14)SLOPE,CEPT
             C
             C******** SUBTRACT EXP FIT FROM PEAK
             C
0122              DO1001 J=NCOMP,IPPUL
0123              VAR(J)=VAR1(J)
0124         1001 SPECT(J)=SPEC1(J)
0125              WRITE(3,15)
0126              DO699 K=IPPLL,IPPUL
0127              EXTRAP=CEPT*EXP(SLOPE*FLOAT(K))
0128              VAR(K)=((SPECT(K)-EXTRAP)**2)/(SPECT(K)+(FLOAT(K))**2)+VAR(K)
0129              SPECT(K)=SPECT(K)-EXTRAP
0130          699 CONTINUE


FORTRAN IV G LEVEL 1, MOD 3            MAIN              DATE = 69080        14/21/40            PAGE 0004

0131          701 WRITE(3,9)
0132              WRITE(3,8)IK,SPECT(K),VAR(K),K=IPPLL,IPPUL)
0133              GOTO142
0134          700 CONTINUE
0135          703 CR=AREAS(1)*AREAS(2)/AREAS(3)+TAREA
0136              WRITE(3,18)AREAS(1),AREAS(2),AREAS(3),TAREA,CR
0137              CR1=CR/WEIGHT
0138              WRITE(3,22)CR1
0139              ALAM=.693/15.
0140              FEE=.693*STIME/15.
0141              FIE=1.-EXP(-FEE)
0142              FOE=ALOG(FIE/FEE)
0143              FUM=FOE*15./.693
0144              TBAR=TR-FUM
0145              WRITE(3,25)TIRR,STIME,TR,TBAR
0146              CRNOT=CR*EXP(ALAM*TBAR)
0147              WRITE(3,24)CRNOT
0148              FLU=CRNOT*26.98*TIRR/(.11525*.602*WEIGHT*(1.-EXP(-ALAM*TIRR))*STIM
                 1E)
0149              SIG1=(CC(1)*AREAS(2)/AREAS(3))**2
0150              SIG2=(CC(2)*AREAS(1)/AREAS(3))**2
0151              SIG3=(AREAS(1)*AREAS(2)*CC(3)/(AREAS(3)**2))**2
0152              SIG2G=SIG1+SIG2+SIG3+TAREA
0153              WRITE(3,29)SIG1,SIG2,SIG3
0154              SIG2F1=(FLU/CR)**2*SIG2G
0155              SIG2F2=(FLU*.00277/.11525)**2
0156              SIG2F=SIG2F1+SIG2F2
0157              WRITE(3,30)SIG2F1,SIG2F2
0158              SIGF=SIG2F**.5
0159              WRITE(3,26)FLU,SIGF
0160          704 CONTINUE
0161              GOTO100
0162              END
```

```
FORTRAN IV G LEVEL 1, MOD 3            GAUSS              DATE = 69080        14/21/40            PAGE 0001

0001              SUBROUTINE GAUSS(SPECT,NCHN,IPPLL,IPPUL,BO,YO,XO,AREA,C,VAR,A,B)
0002              DIMENSIONSPECT(256),A(3,3),B(3),C(6),B2(30),BKG(256),VAR(30)
0003            4 FORMAT(35H LOWER LIMIT OF PHOTOPEAK FROM CHAN,I4,8H TO CHAN,I4,/
                 1,35H UPPER LIMIT OF PHOTOPEAK FROM CHAN,I4,8H TO CHAN,I4)
0004            9 FORMAT( //30H EXPERIMENTAL PHOTOPEAK POINTS /  )
0005           10 FORMAT( //28H CALCULATED PHOTOPEAK POINTS /  )
0006           14 FORMAT(// 18H FUNCTION ERROR = ,E14.8,5X,11HLN ERROR = ,E14.8/)
0007           15 FORMAT( 1X,5E16.8 )
0008              F(X)=YO*EXP(-((X-XO)**2)/BO)
0009              IPPLO=IPPLL
0010              IPPUO=IPPUL
0011          212 XN=0.
0012              DO 20 I=1,3
0013              B(I)=0.
0014              DO 20 J=1,3
0015           20 A(I,J)=0.
                C**** FORM SOLUTION MATRIX
0016              DO 30 I=IPPLL,IPPUL
0017              XN2=XN*XN
0018              XN3=XN2*XN
0019              XN4=XN3*XN
0020              ZN=ALOG(SPECT(I))
0021              A(1,1)=A(1,1)+XN4*VAR(I)
0022              A(1,2)=A(1,2)+XN3*VAR(I)
0023              A(1,3)=A(1,3)+XN2*VAR(I)
0024              A(2,3)=A(2,3)+XN*VAR(I)
0025              A(3,3)=A(3,3)+VAR(I)
0026              B(1)=B(1)+XN2*ZN*VAR(I)
0027              B(2)=B(2)+XN*ZN*VAR(I)
0028              B(3)=B(3)+ZN*VAR(I)
0029           30 XN=XN+1.
0030              A(2,1)=A(1,2)
0031              A(3,1)=A(1,3)
0032              A(2,2)=A(1,3)
0033              A(3,2)=A(2,3)
0034              CALL INVERT(3,A,8)
0035              XO=(-B(2)/(2.*B(1)))
0036              BO=-1./B(1)
0037              Y1=0.
0038              Y2=0.
0039              XN=0.
0040              DO 104 I=IPPLL,IPPUL
0041              Y1=Y1+EXP(-(XN-XO)**2/BO)
0042              Y2=Y2+EXP(-2*(XN-XO)**2/BO)/SPECT(I)
0043          104 XN=XN+1.0
0044              YO=Y1/Y2
0045              C(3)=1./Y2
0046              XO=XO+FLOAT(IPPLL)
0047              N=0
0048              RES=0.
0049              STDEV=0.
0050              XN=0.0
0051              DO 40 I=IPPLL,IPPUL
0052              STDEV=STDEV+((ALOG(SPECT(I))-B(3)-B(2)*XN-B(1)*XN**2)**2)
0053              RES=RES+(SPECT(I)-F(FLOAT(I)))**2
0054           40 XN=XN+1.
0055              WRITE(3,14)RES,STDEV
0056              STDEV=SQRT(RES/FLOAT(IPPUL-IPPLL-2))
```

```
FORTRAN IV G LEVEL 1, MOD 3            GAUSS              DATE = 69080        14/21/40            PAGE 0002

0057              IF(1.5*STDEV.GT.ABS(SPECT(IPPLL)-F(FLOAT(IPPLL))))GO TO 50
0058              IPPLL=IPPLL+1
0059              N=1
0060           50 IF(STDEV.GT.ABS(SPECT(IPPUL)-F(FLOAT(IPPUL))))GO TO 60
0061              IPPUL=IPPUL-1
0062              N=1
0063           60 IF(N.EQ.1) GO TO 212
0064              SIG=SQRT(BO)
0065              AREA=YO*SQRT(3.14159)*SIG
0066              IF(IPPLO.NE.IPPLL) GO TO 70
0067              IF(IPPUO.EQ.IPPUL)GO TO 71
0068           70 WRITE(3,4) IPPLO,IPPLL,IPPUO,IPPUL
0069           71 ZN=1./(4.*B(1)**2)
0070              XN=(B(2)/B(1))**2
0071              XN2=1./(B(1)**4)
0072              XN3=XN/4.
0073              XN4=(XN**2)/FLOAT(NCHN)
0074              C(1)=ZN*(A(2,2)+XN*A(1,1))
0075              C(2)=XN2*A(1,1)
0076              C(4)=0.6922*C(2)/BO
0077              C(5)=((C(4)+C(1)*2.7689*BO/(XO**2))/(XO**2))
0078              C(6)=3.1416*(BO*C(3)+C(2)*YO**2/(4.*BO))
0079              DO 100 I=1,6
0080          100 C(I)=SQRT(C(I))
0081              C(5)=100.*C(5)
0082              MAX=IPPUL-IPPLL+1
0083              XN=0.
0084              XO=XO-FLOAT(IPPLL)
0085              DO 105 I=1,MAX
0086              B2(I)=F(XN)
0087          105 XN=XN+1.
0088              XO=XO+FLOAT(IPPLL)
0089              WRITE(3,9)
0090              WRITE(3,15)(SPECT(I),I=IPPLL,IPPUL)
0091              WRITE(3,10)
0092              WRITE(3,15)(B2(I),I=1,MAX)
0093              RETURN
0094              END
```

```
0001              SUBROUTINE INVERT(NISO,R,B)
0002              DIMENSION R(3,3),RI(3,3),C( 6),B(3)
                  C
                  C        INVERT RESPONSE MATRIX BY BORDERING METHOD
                  C
0003              R(1,1)=1./R(1,1)
0004              ISO = 1
0005            120 ISO=ISO+1
0006              MAX=ISO-1
0007              ANN=0.
0008              DO 110 J=1,NISO
0009              DO 110 I=1,NISO
0010            110 RI(I,J)=0.
0011              DO 101 I=1,MAX
0012            101 C(I)=R(I,ISO)
0013              DO 102 J=1,MAX
0014              DO 102 I=1,MAX
0015            102 ANN=ANN+  C(I)*R(I,J)*C(J)
0016              RI(ISO,ISO)=1./(R(ISO,ISO)-ANN)
0017              DO 103 J=1,MAX
0018              DO 103 I=1,MAX
0019              RI(J,ISO)=RI(J,ISO)-R(J,I)*  C(I)*RI(ISO,ISO)
0020              RI(ISO,J)=RI(J,ISO)
0021              DO 103 K=1,MAX
0022              DO 103 L=1,MAX
0023            103 RI(I,J)=RI(I,J)+R(I,L)*  C(L)*  C(K)*R(K,J)
0024              DO 104 I=1,MAX
0025              DO 104 J=1,MAX
0026            104 RI(I,J)=RI(I,J)*RI(ISO,ISO)+R(I,J)
0027              DO 105 I=1,ISO
0028              DO 105 J=1,ISO
0029            105 R(I,J)=RI(I,J)
0030              IF(ISO.LT.NISO) GO TO 120
0031              DO 106 J=1,NISO
0032              C(J)=0.0
0033              DO 106 I=1,NISO
0034            106 C(J)=C(J)+R(J,I)*B(I)
0035              DO 107 I=1,NISO
0036            107 B(I)=C(I)
0037              RETURN
0038              END
```

THE RESPONSE OF ^{6}LiF AND ^{7}LiF THERMOLUMINESCENT DOSIMETERS TO NEUTRON AND GAMMA-RADIATION DOSE

by

CHARLES EDWARD BLISS

B. S., Kansas State University, 1967

AN ABSTRACT OF A MASTER'S THESIS

submitted in partial fulfillment of the

requirements for the degree

MASTER OF SCIENCE

Department of Nuclear Engineering

KANSAS STATE UNIVERSITY
Manhattan, Kansas

1969

ABSTRACT

Theory of thermoluminescence and thermoluminescent dosimetry was reviewed. Factors affecting the thermoluminescent response of LiF were discussed. The theory of foil activation as a means of fluence determination using the sum peak method to determine absolute activity was discussed.

A postirradiation annealing procedure of 7 minutes at 110°C followed by readout 24 hours later was found experimentally to reduce problems of fading in EG and G model TL-22 and model TL-23 thermoluminescent dosimeters.

Calibration curves for ^{60}Co gamma radiation in the dose range (10^2 to 6×10^3) R were determined for both dosimeter types. Calibration curves for 14.7 MeV neutrons in the fluence range ($.6 \times 10^{11}$ to 60×10^{11}) neutrons/cm^2 were obtained. Correlation curves for equivalent response plotting ^{60}Co dose vs. fluence were also obtained.

Conclusions drawn from analysis of the data were:

(1) the postirradiation process has a different effect on ^6LiF and ^7LiF thermoluminescent dosimeters;

(2) gamma-ray irradiation of both ^6LiF and ^7LiF TLD's followed by postirradiation annealing results in lower-temperature traps, while neutron irradiation followed by postirradiation annealing does not result in lower-temperature traps;

(3) the response of ^7LiF TLD's to 14.7 MeV neutrons is lower by about 20% than the response of ^6LiF TLD's to an equivalent neutron dose;

(4) on a tissue dose basis, TL-22 dosimeters are approximately 6.2 times as sensitive to ^{60}Co gamma rays as to 14.7 MeV neutrons, while TL-23 dosimeters are about 7.7 times as sensitive to ^{60}Co gamma rays as to 14.7 MeV neutrons;

(5) in a mixed radiation field of 14.7 MeV neutrons and ^{60}Co gamma rays, the presence of populated traps created by one type of radiation does not affect the creation of populated traps by the other type of radiation in either ^{6}LiF or ^{7}LiF.